NUMERICAL ANALYSIS OF COMPRESSION PERPENDICULAR TO THE GRAIN IN GLULAM BEAMS WITH AND WITHOUT REINFORCEMENT

JIMMY PERSSON

Structural
Mechanics

Master's Dissertation

NUMERICAL ANALYSIS OF COMPRESSION PERPENDICULAR TO THE GRAIN IN GLULAM BEAMS WITH AND WITHOUT REINFORCEMENT

Master's Dissertation by
JIMMY PERSSON

Supervisors:
Per Johan Gustafsson *Professor*,
Div. of Structural Mechanics, LTH, Lund

Roberto Crocetti *Professor*,
Div. of Structural Engineering, LTH, Lund

Examiner:
Kent Persson *PhD*,
Dept. of Construction Sciences, LTH, Lund

Abstract

In Sweden there has recently been a change in the code from the former BFS2010:2 BKR 13 to Eurocode 5. This shift has led to changes when calculating the design capacity for all materials including wood. One of the parameters that were changed was the strength of wood perpendicular to the grain. The characteristic value required was decreased from 8 MPa to 2.7 MPa which have a relativity large impact on the size of the contact area, for instance between a beam and a support. A consequence of this is that the support has to be larger and in many situations more expensive. Discussions with SWECO Structures, the Division of Structural Engineering and the Division of Structural Mechanics led to to believe that the decrease in characteristic capacity is not fully motivated for all loading situations. Besides the evaluation of the decrease, an investigation of how reinforcement in form of wooden dowels and threaded steel screws affect the compression capacity perpendicular to the grain.

The analysis of the compression capacity perpendicular to the grain, with and without reinforcement, is based on analytical models and by means of numerical calculations by a Finite element program called ABAQUS. To capture the plastic non linear behavior perpendicular to the grain two material models were combined, one which handles the stress in longitudinal direction and one handling the stresses in radial and tangential directions. Parallel to this thesis another Master's thesis is produced with the same objective but by a different method, laboratory testings. This is advantageous since it makes it possible to judge the creditability of the FE-models.

A total number of 16 FE-models were produced with different loading situations and setups to investigate how the support length and reinforcement effect the stress capacity perpendicular to the grain. When it was evident that the unreinforced models captured the real behavior 4 new models were produced with support length 100-400 mm to see how the stiffness, maximal capacity and deformations depends on the support length.

The results of the unreinforced FE-models show that the decrease from 8 MPa to 2.7 MPa is motivated in some cases where small deformations only are acceptable and with a support length $\geq$ 400 mm. However, if a deformation of 20 mm is acceptable and the support length is 100 mm, the compression capacity is above 8 MPa according to the FE-results.

The FE-models handling wooden dowels captured the behavior very well in the elastic area when comparing the models with laboratory tests. When the specimen began to crack the dowels buckled. This phenomenon has not been taken into account in this thesis since it is complicated and time consuming modeling crack propagation. The models with threaded steel rods were difficult to model even in the elastic area due to the fact that the reinforcing rods were irregularly pushed in from the bottom side of the beam. The result shows that there is an advantage in stiffness if the rods are in flush with the bottom side of the beam because they could take load simultaneously. The mean capacity for the supports with wooden dowels was calculated to 11 MPa and for the threaded steel rods 15 MPa compared to 5 MPa unreinforced.

Sammanfattning

I Sverige har nyligen byggkonstruktionsnormen förändrats från den föregående normen BFS 2010:2 BKR 13 till Eurocode 5. Reformen har lett till förändringar vid beräkningar av dimensionerande lastkapacitet för alla material inkluderat trä. En av parametrarna som förändrats för trä är hållfastheten vid tryck vinkelrätt fibrerna. Det karakteristiska värdet 8 MPa sänktes till 2.7 MPa vilket har en relativt stor inverkan på erforderlig storlek av kontaktytan mellan till exempel en balk och ett upplag. En konsekvens av detta är att kontaktytan måste förstoras och i många situationer leder till en dyrare konstruktion. Diskussioner med SWECO Structures, avdelningen för Konstruktionsteknik och avdelningen för Byggnadsmekanik ledde till att det finns anledning att tro att sänkningen av det karakteristiska värdet inte är motiverat för alla lastsituationer. Förutom utredning av sänkning av karakterisiskt värde görs en undersökning huruvida förstärkning i form av trädymlingar och gängade stålstavar påverkar tryckkapaciteten vinkelrätt fiberriktningen.

Analysen är baserad på analytiska modeller för att beräkna tryck vinkelrätt fiberriktningen med och utan förstärkning samt på numeriska modeller i ett Finita elementprogram, ABAQUS. För att fånga det plastiska olinjära beteendet vinkelrätt fiberriktningen har två stycken materialmodeller kombinerats, en som fångar spänningarna i longitudinell riktning och en som fångar spänningarna i radiell och tangentiell riktning. Parallellt med denna studie har ett examensarbete gjorts med samma mål men med hjälp av laborationer. Detta är fördelaktigt för då finns möjligheten att avgöra hur verklighetsnära FE-modellerna är.

Totalt skapades 16 FE-modeller med olika belastningssituationer och förutsättningar för att undersöka hur upplagslängder och förstärkningar påverkar tryckkapaciteten vinkelrätt fiberriktningen. När det visade sig att de oförstärkta modellerna fångande beteendet i verkligheten skapades följaktligen 4 nya modeller med upplagslängder 100-400 mm för att se hur styvhet, maximal kapacitet och deformationer beror på upplagslängd.

Resultatet av de oförstärkta FE-modellerna visar att sänkningen från 8 MPa till 2.7 MPa är motiverat i fall då endast små deformationer är tillåtna och vid upplagslängd $\geq$ 400 mm. Men om en deformationsmagnitud på 20 mm är tillåten och upplagslängden är 100 mm så är tryckkapaciteten vinkelrätt fiberriktningen 8 MPa enligt FE-resultaten.

De förstärkta FE-modellerna som modelerade trädymlingarna fångade det verk-

liga beteendet mycket bra under elastiska förhållanden. När provbalkarna började
spricka knäcktes dymlingarna. Detta fenomen har inte medtagits i denna studie
då sprickbildning är komplext och tar lång tid att modellera. Modellerna med gän-
gade stålstavar var svåra att modellera även under elastiska förhållanden. Detta
beror på att stålstavarnas placering från underkant balk var mycket oregelbun-
den. Dessa modeller visar dock att det finns en fördel i form av ökad styvhet om
stavarna placeras i jämnhöjd med balkens undersida då alla stavar kan ta last sam-
tidigt. Medelvärdeskapaciteten för trädymlingarna beräknades till 11 MPa och för
stålstavarna 15 MPa att jämföra med 5 MPa utan förstärkning.

Preface

This Master's thesis work was carried out at the Division of Structural Mechanics at Lund Institute of Technology as a conclusion to my Master's degree in Civil Engineering. The work has been carried out during the summer of 2011.

First I would like to thank my supervisors professor Per Johan Gustafsson at the Division of Structural Mechanics and professor Roberto Crocetti at the Division of Structural Engineering for their great guidance and support during this work. Without their help this thesis could not have been done. A special thank goes to Kent Persson at the Division of Structural Mechanics for his deep knowledge about ABAQUS, Mikael Rosengren who provided starting models and to the fellow students I shared office with for interesting and helpful discussions.

I would also like to thank Magnus Persson at SWECO Structures for his guidance and patience during these years, Ildigo Lang at Epsilon who worked as my career mentor and my former colleagues at Lunicore Student Consulting for their contagious dedication and entrepreneurship.

Finally I would also like to express my deepest gratitude and love to my parents Dag and Gunilla for their great support and decisive engagement during my entire education.

Jimmy Persson
Lund, August 2011

Notations

General notations

$(\dot{\ })$	time differentiation of ( )
$\tilde{\nabla}$	matrix differential operator
$[\ ]^T$	transpose of a matrix
$[\ ]^{-1}$	inverse of a matrix
$\displaystyle\int_S (\ )\,dS$	integration over surface
$\displaystyle\int_V (\ )\,dV$	integration over volume
$\displaystyle\sum (\ )$	sum of ( )

Roman upper case letters

A	contact area
A_{ef}	effective contact area
$\mathbf{D}$	constitutive matrix in the global coordinate system
E	Youngs modulus
E_L	Youngs modulus, longitudinal
E_R	Youngs modulus, radial
E_T	Youngs modulus, tangential
F	Load
G_{LR}	shear module, longitudinal-radial
G_{LR}	shear module, longitudinal-tangential
G_{LR}	shear module, radial-tangential
$\mathbf{K}$	stiffness matrix
$\mathbf{N}$	shape function matrix
$\mathbf{u}$	displacement vector
$\mathbf{D}$	constitutive matrix in the global coordinate system
V	volume

Roman lower case letters

$\mathbf{a}$	column matrix of nodal displacements
a	distance to the beam edge
b	beam width
h	beam height
h_{reinf}	reinforcement length
l	length
l_{eff}	effective length
$l_{support}$	support length
$\mathbf{t}$	traction vector
$\mathbf{u}$	displacement vector
$\mathbf{v}$	vector of weight functions

Greek letters

α	angle in radians
$\boldsymbol{\epsilon}$	strain vector
ϵ	strain
δ	displacement
ν	Poissons ratio
ν_{LR}	Poissons ratio, longitudinal-radial
ν_{LT}	Poissons ratio, longitudinal-tangential
ν_{RT}	Poissons ratio, radial-tangential
$\boldsymbol{\sigma}$	stress vector
$\sigma_x\,\sigma_y\,\sigma_z$	normal stresses in x, y and z-direction

Contents

Chapter 1

Introduction

1.1 Background

Wood is a material with great potential since the raw material from which it is obtained is cheap, environmentally friendly and represents renewable material. Historically, wood as a material has been used for multiple uses. From making spears 40,000 years ago, as a construction material to build boats and bridges with the Middle Ages until today when wood is used to make large glulaminated beams serving as frame systems in ice rinks and multi-story buildings. In order for the buildings not to collapse, the design of a structural system is controlled by codes which differ in each country.

In Sweden there has recently been a change in the code from BKR to Eurocode 5. This shift has led to changes when calculating the design capacity for all materials including wood. One of the parameters that were changed was the characteristic strength perpendicular to the grain, which has been decreased from 8 MPa to 2.7 MPa for glulaminated timber (corresponding class L40). This parameter has a large impact on the contact area at a support. The decrease from 8 MPa to 2.7 MPa implicates that the contact area must be larger, according to the code, to distribute the load and reduce the stress level. This leads to design problems, e.g. the cost of a larger support area, for instance a larger column cross section. Another problem if a joinst hanger is being used is an increase of eccentricity and therefore a torsional moment at the axis of a supportive beam.

The strength perpendicular to the grain occurs at contact surfaces between two or more elements. The capacity is determined by two parts: crushing of the fibers and unloaded length. Unloaded length implies that the stress is transported to the neighboring unloaded parts (of a beam for instance) and is treated different depending on which code is being used. In the Eurocode there is an increase factor, k_c, which takes load distribution into account. If the support length is lower than a specific value (400 mm) and the load is located at a certain distance from the support (2 x h_{beam}) the perpendicular capacity can be increased with

1

a factor 1.75. Discussions with SWECO Structures, the Division of Structural Engineering and the Division of Structural Mechanics (both divisions at Lund Institute of Technology) led to there is reason to believe that the coefficient varies with different support lengths below 400 mm.

Another aspect of strength perpendicular to the grain is when wood reaches high stresses perpendicular to the grain the material goes from elastic behavior into ductile plastic. To increase the elastic behavior and the maximum stress capacity perpendicular to the grain there will be an investigation how wood and steel reinforcement can affect the capacity. There are several benefits with wood reinforcement for instance economical ones.

1.2 Aim

In this thesis, the following aims apply:

- Gain knowledge about wood as an orthotropic construction material.

- Identify models of how to calculate the stress perpendicular to the grain (with and without reinforcement).

- Identify differences between the former Swedish building code BKR 13 and the newly adopted Eurocode 5 for calculating the compressive strength perpendicular to the grain (with and without reinforcement).

- Produce a working Finite element method (FEM) model which captures both the elastic and the plastic behavior of wood when stressed perpendicular to the grain.

- Identify how the compressive stress capacity in wood is affected by support length at supports lengths less than 400 mm.

- Produce a simple calculation method for the increase factor k_c for support lengths below 400 mm.

- Identify the effect of wood and steel as reinforcement in stress perpendicular to grain for three different setups with different geometry and number of screws.

1.3 Method

A theory study is made to gain knowledge about wood as a construction material and its orthotropic behavior. Analyzes of the stiffness properties relationship is made to illuminate the different capacity in different directions.

Identification of models and the difference in building codes is done by reviewing articles, reports and the building codes, Eurocode 5 and BFS 2010:2 BKR 13. For illustrating the differences an example is calculated and plotted with different support lengths.

ABAQUS is a Finite element program with several of different material models for capturing very many materials behavior. In this thesis a foam hardening will be used to capture the plastic behavior of wood perpendicular to the grain. To prove the FEM-models creditability the models are compared to lab tests which have been made parallel to this Master's thesis. The comparisons are made in stress-deformation plots.

Analyze of how the stress perpendicular to the grain behaves below 400 mm is done by observing the plots from the FEM-models. From four different support length plots it is possible to produce a simple method for calculating the increase factor k_c by defining a specific deformation requirement.

The reinforced beams are modeled in ABAQUS and the results are plotted in a stress-deformation plot to compare the reinforced beam results with the unreinforced beams.

1.4 Limitations

In the work process, following limitations apply:

- The deformation perpendicular to the grain is studied, not the possible risk for splitting due to compressive stresses.

- Climate class 1.

- The woods moisture content is constant across the cross section and about 12 %.

- The material is modeled as a homogeneous material which means, for instance, knots and difference between spring wood and autumn wood will not be taken into account.

- Crack propagation will not be studied.

- The annual rings will not be modeled nor the difference in lamellas in each beam.

- The Finite element models in ABAQUS are modeled in 3D with the assumption transversely isotropic material property.

- The report will focus on what is happening around the support locally.

- The analysis and calculations will be focused on compression perpendicular to the grain and the reinforcement.

- Non linear geometry/large deformation-theory will be used in numerical calculations.

- All models have been created in SI-units.

1.5 Outlines

This thesis is mainly divided into three parts:

The first part contains chapter 2-4 to get a deeper knowledge of wood as a construction material and its mechanical attributes. Chapter 2 contains a description of wood as a construction material, its orthotropic behavior and stiffness properties. Glue laminated beams are presented and explained. Chapter 3 introduces the compression perpendicular to the grain and some explanations of previous work in this area. Later in chapter 3 a comparison is made between some of the different codes in Europe. To get a better understanding how reinforcement perpendicular to the grain in beams work, a shorter theory study and a comparison with different theories is made in chapter 4.

Second part includes a short presentation of the laboratory tests which have been made parallel to this thesis in chapter 5. Chapter 6 is dedicated to explain how the Finite element method (FEM), a numerical calculation method, works in short. The FE-models of the unreinforced beams are handled in chapter 7. Assumptions and model properties are presented as well as the results. Finally an analysis of the increase factor $k_{c,90}$ is made. Chapter 8 is structured in the same way, just this chapter handles the reinforced beams.

The third and final part, chapter 10, contains overall conclusions to this thesis. In this part there are also suggestions for future work regarding this subject which have to be investigated further.

Chapter 2

Introduction to wood as a construction material

In this chapter an introduction to wood as a construction material is made. First the orthotropic behavior is described and later the elastic stiffness properties. Thereafter a short introduction to non linear behavior in different directions and finally a short presentation of glulaminated beams.

2.1 An orthtropic material

Wood is an anisotropic material with some structural symmetry, both in microscopic and macroscopic view. The heterogeneous structure of annual rings leads however to asymmetry because of altering spring- and autumn wood (which varies in growth in different years). Another important aspect which leads to inexact heterogeneous structure is a various forms of defects of development, for example twigs and distorted fibers [10].

Since a tree grows in a cylindrical manner, the different properties of wood can be related to the tree principal directions of growth. Many of the woods properties i.e. strength and elasticity depends on this cylindrical symmetry. A very small cube cut out a piece from the core has three orthogonal symmetry planes: L, R and T, as shown in *figure 2.1*. L answers for the direction parallel to the fibers, R is the direction perpendicular to fibers and radius to the annual rings and finally T is the direction perpendicular to the fibers tangential to the annual rings [7].

A material is said to be orthotropic if there are three symmetry planes mutually perpendicular to each other in every point in the material. Symmetry exists if two coordinate systems, which are mirror images of each other with respect to this plane, leave the material matrices unchanged [13]. The three planes in wood which normally fulfills this symmetry requirement are the planes that have normal vectors in the longitudinal, radial and tangential directions. Therefore wood will
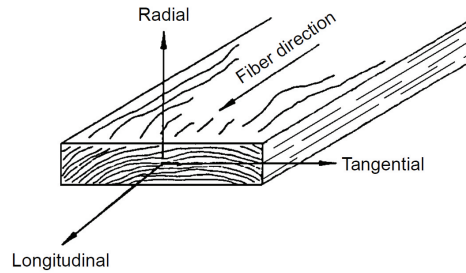
Figure 2.1: Principal axes of wood with respect to grain direction and growth rings.[10]

be handled as an orthotropic material in this thesis. Yet, this assumption is only valid when looking into wood in a non macroscopic view and the tensions must be small so elastic conditions apply [10].

2.2 Stiffness properties

The mechanical properties of wood depends on several different factors, like temperature, density, moisture content, angle of microfiber contra their cell wall, angle of loading contra direction of fiber, time under loading (creep, relaxation, fatigue) etc. When a piece of wood is exposed to stress, which is lower than its yield strength, the body behaves as an elastic orthotropic material. When the stress magnitude exceeds the yield point, the material enters a plastic behavior. Plastic behavior is characterized by the stress no longer is proportional to the strain which will be discussed later on in this chapter.

2.2.1 Linear elasticity

Below the limit of proportionality wood can be described with Hooke's generalized law. For linear elasticity in one dimension

$$\sigma = E\epsilon \tag{2.1}$$

where E is a module of elasticity (material dependent) and epsilon represents strain. In reality there are other variables such as moisture-induced shrinkage, mechano-sorptive deformation and creep deformation [15]. This will not be handled in the present study. Partly due to it is time consuming but also because the effect of mentioned variables have little effect in short-time loading.

Because of the constitutive behavior in the elastic region *equation 2.2* can be generalized in three dimensions:

$$\boldsymbol{\sigma} = \mathbf{D}\boldsymbol{\epsilon} \tag{2.2}$$

6

where

$$
\boldsymbol{\sigma} = \begin{bmatrix} \sigma_{11} \\ \sigma_{22} \\ \sigma_{33} \\ \sigma_{12} \\ \sigma_{13} \\ \sigma_{23} \end{bmatrix} \qquad \mathbf{D} = \begin{bmatrix} D_{11} & D_{12} & \ldots & D_{16} \\ D_{21} & D_{22} & \ldots & D_{26} \\ \vdots & \vdots & \ddots & \vdots \\ D_{61} & D_{62} & \ldots & D_{66} \end{bmatrix} \qquad \boldsymbol{\epsilon} = \begin{bmatrix} \epsilon_{11} \\ \epsilon_{22} \\ \epsilon_{33} \\ \epsilon_{12} \\ \epsilon_{13} \\ \epsilon_{23} \end{bmatrix} \tag{2.3}
$$

I.e. the D-matrix is the stiffness matrix. Handling linear elastic materials the stiffness matrix has to be constant for a given position. Additionally, the matrix has to be positive definite and invertible.

$$
\boldsymbol{\epsilon} = \mathbf{C}\boldsymbol{\sigma} \tag{2.4}
$$

where $C = D^{-1}$. The elasticity defined by $\epsilon = C\sigma$, which possess properties if linearity and one to one relation between stresses and strains, is also termed Cauchy elasticity. If, in addition to these properties, the strain energy for a given strain state only depends on the strain rate itself and not the manner in which this strain state was obtain the material is hyperelastic. By hyperelasticity follows that the D-matrix is symmetric which leads to the numbers in the stiffness matrix can be reduced from 36 coefficients to 21. Assuming elastic orthogonality reduces further from 21 to 9 different coefficients. Using Hook's generalized law an orthotropic material can be written by use of matrix notation as:

$$
\begin{bmatrix} \epsilon_{LL} \\ \epsilon_{RR} \\ \epsilon_{TT} \\ \gamma_{LR} \\ \gamma_{LT} \\ \gamma_{RT} \end{bmatrix} = \begin{bmatrix} \frac{1}{E_L} & \frac{-\nu_{RL}}{E_R} & \frac{-\nu_{TL}}{E_T} & 0 & 0 & 0 \\ \frac{-\nu_{LR}}{E_L} & \frac{1}{E_R} & \frac{-\nu_{TR}}{E_T} & 0 & 0 & 0 \\ \frac{-\nu_{LT}}{E_L} & \frac{-\nu_{RT}}{E_R} & \frac{1}{E_T} & 0 & 0 & 0 \\ 0 & 0 & 0 & \frac{1}{G_{LR}} & 0 & 0 \\ 0 & 0 & 0 & 0 & \frac{1}{G_{LT}} & 0 \\ 0 & 0 & 0 & 0 & 0 & \frac{1}{G_{RT}} \end{bmatrix} \begin{bmatrix} \sigma_{LL} \\ \sigma_{RR} \\ \sigma_{TT} \\ \tau_{LR} \\ \tau_{LT} \\ \tau_{RT} \end{bmatrix} \tag{2.5}
$$

In the matrix C above there are nine independent parameters which describe the stiffness of the orthotropic material: three moduli of elasticity, three moduli of shear (also called rigidity) and three moduli of Poissons ratio. The moduli of elasticity (E_L, E_R and E_T) are the elastic modulus along the longitudinal, radial and tangential axes and are often obtained from compression tests. The shear moduli (G_{LR}, G_{LT} and G_{RT}) indicate the resistance to deflection of a member caused by shear stress. Poissons ratio is the ratio of the transverse to axial strain and is denoted by (V_{RL}, V_{TL} and V_{TR}). The first letter of the subscript refers to the direction of the applied stress and the second letter to direction of lateral deformation [7].

2.2.2 Non linear elasticity

When wood is loaded to higher stress levels, plastic deformation or failure occurs. Plastic deformation is a non linear-behavior and occurs when a material is utilized for stress above its yield point, see *figure 2.2*. In this stage plastic deformation occurs which are not reversible and therefore permanent even when the material is unloaded [14].
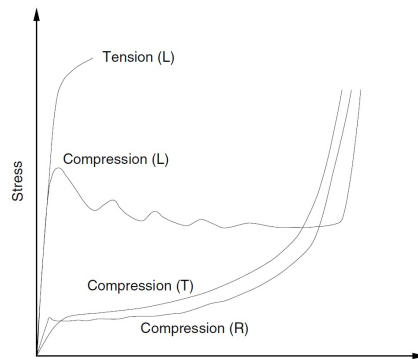
Figure 2.2: Typical stress-strain curves for wood loaded in compression in the longitudinal, radial and tangential directions and for tension in the longitudinal direction [16].

2.3 Glulaminated timber (Glulam)

The development of Glulam technology was initiated in Germany during the late 19th century. The technology became known in Norway, who introduced it to Scandinavia in the beginning of the 20th century. The first laminated structure in Sweden was manufactured in Töreboda 1918. Most of the produced laminated wood is used for industrial buildings, residential buildings and others but also for bridges and parking garages. Glulam beams can be produced with very long span and practically speaking, it is usually the transport options that limit the range. The consummation in Sweden is an average of 30,000 cubic meters a year [2].

A glulam cross-section is built up with parts of similar strength, homogeneous wood. To optimize the timber's strength timber of higher quality can be used in the cross-sections outer parts, see *figure 2.3*. This is because it is often where the stresses are greatest. Glulam elements, like common wood characteristics in terms of the strength, vary in different directions (L,R,T), humidity and load duration reduces strength and is also an highly inhomogeneous material. However, compared with an ordinary beam a glulam beam has higher strength properties due to the so-called lamellae's effect. This effect can be briefly explained that the lamellae with different characteristics are mixed and therefore the risk of serious errors (for instance knots) to occur in the same cross section is small [2].
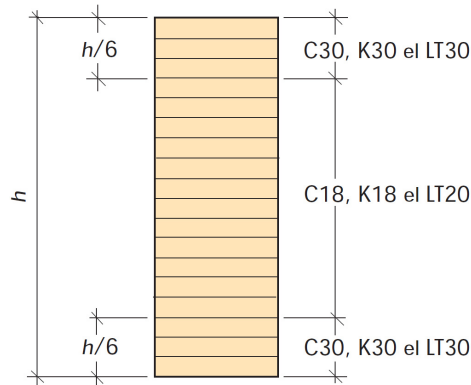
Figure 2.3: Construction of a glulaminated heterogeneous cross-section [2].

Chapter 3

Compression perpendicular to the grain

This chapter starts with a general introduction looking where compression perpendicular to the grain occurs and what failure modes accompanying these setups. It is followed by a review of an article dealing with the effect of unloaded length generally and an article handling unloaded length with high cross sections. Further the former Swedish code BFS 2010:2 BKR13 is presented as well as Eurocode 5. The chapter ends with a calculation to compare the differences in the codes.

3.1 General introduction

Contact joints where loads are introduced by compression perpendicular to the grain are easy to produce and assemble and therefore widely used in timber structures. Some examples of usual connections where wood is subjected to stress perpendicular to the grain can be seen in *figure 3.1*.

Contrary to most types of timber connection, the load deformation behavior of contact joints is generally very ductile and does not develop a brittle failure mechanism, considering ultimate limit state. But it leads to high levels of unfavorable deformations which could lead to the structural system out of serviceability limit state. When wood fail as a material, one mode of failure is when a line of cell walls collapse. The wall collapse where the weakest cells are placed and buckling failure of cells are achieved due to radial compression stress, see *figure 3.2*. Another mode of failure is where a local compressive force acts on a small area of the wood. A third mode of failure is when the wood is exposed to shearing by the annual rings, see *figure 3.2*. This phenomenon might occur in trusses where the beams are joined by nail plates [11].

The capacity in compression perpendicular to the grain is at highest when wood is subjected to load in radial compression to the annual rings and weakest at com-
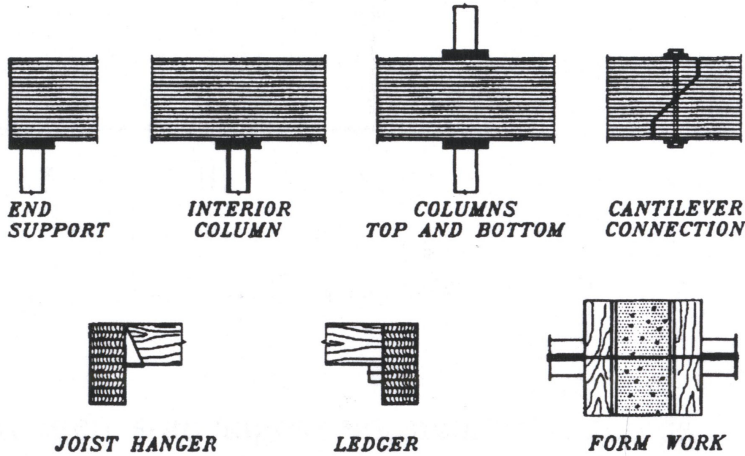
Figure 3.1: Some examples where stress perpendicular to the grain occur [11].

pression at an angle of 45 degrees between the annual rings and the force direction. This is illustrated in *figure 3.3* where compression tangential to the annual rings also is observed.

However, due to woods orthotropic structure, it is difficult to make a general mode of failure for each plane (radial and tangential). This is because in practical use, a force is seldom applied in the tangential or the radial direction. To get a value for the elastic module in compression perpendicular to the grain, E_{90}, a representative mean value has been chosen. It is of interest to notice that (in opposition to tension) imperfections in the timber do not reduce the strength perpendicular to the grain. In fact, sometimes a knot could limit the deformations.
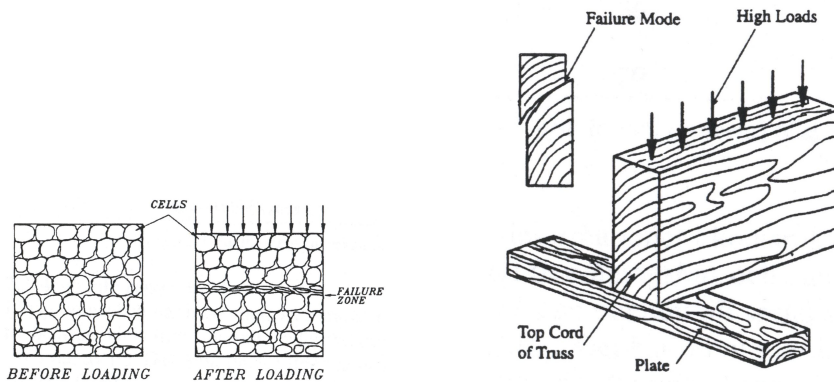
Figure 3.2: Cell buckling to the left and shearing by a annual ring to the right [11].
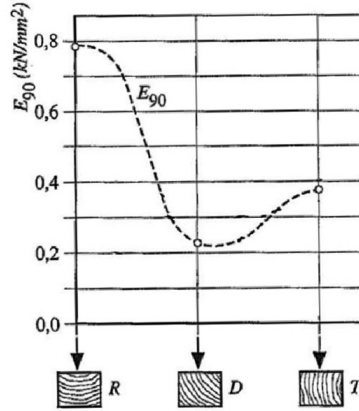
Figure 3.3: Wood in compression perpendicular to the grain. The stiffness can be read from different loading directions [3].

3.2 Definition of the load carrying capacity

The definition of load carrying strength is primary divided into two different definitions: definition by American Society for Testing and Materials (ASTM) and by European Committee for Standardization (CEN). The definition according to both ASTM and CEN is shown in *figure 3.4*. For CEN method the following iterative procedure is considered:

To determine the value of maximum load, $F_{c,90}$, an estimation of maximum load, $F_{c,90,est}$, is done as a first step. Then by calculating $0.1F_{c,90,est}$ and $0.4F_{c,90,est}$ a linear line can be drawn through the intersection points of these values, see line 1 in *figure 3.4*. Parallel to line 1 another line, line 2, is drawn shifted $0,01h$ (where h is the specimen height) to the right on the horizontal axis. In the graph where line 2 intersects the load-deformation curve of tested specimens a value $F_{c,90}$ can be obtained. If the value is within range of 5 % of the estimated value, $F_{c,90,est}$, the procedure ends. Otherwise, the procedure is repeated until the value of $F_{c,90,est}$ is within the tolerance limit [21].
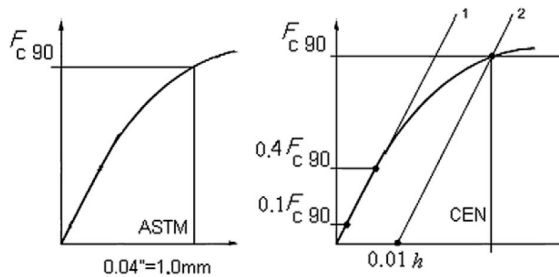
Figure 3.4: Compression strength definition according to ASTM (left) and CEN (right). The horizontal axis represents the specimen deformation [11].

3.3   The effect of unloaded length

A compilation of Suensons tests 1938 made by Edlund in step 1 [3] shows the difference in compression perpendicular to the grain with different test setups. Five different setups are shown in *figure 3.5*, each with a different length. The upper loaded surface is $15x15\ cm^2$ in all setups.
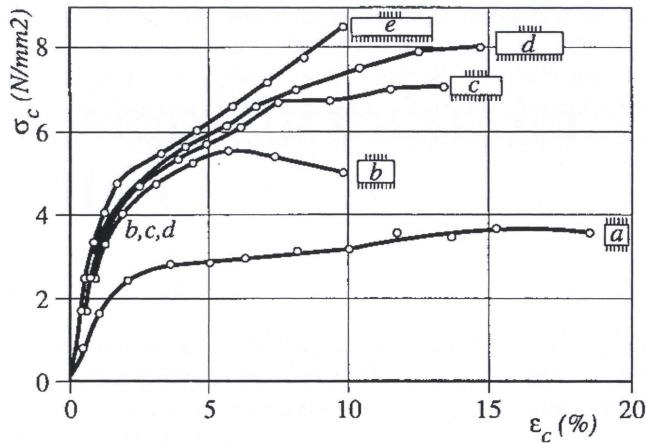
Figure 3.5: Applied stress perpendicular to the grain with different lengths made by Suenson 1938 [3].

Case a)	In this case, the whole element is loaded. The fibers are crushed when the stress reaches the element yield stress. When the yield stress is reached is a significant increase of the deformation can be observed but only small changes in load.
Case b)	When only part of the element is subjected to load, the stiffness will be higher. This is due to the concentrated load will be transferred through the fibers to the neighboring unloaded parts.
Casel c,d,e)	In these cases, the unloaded length is increased further. What can be seen at an increase is a higher stress level is achieved compared to deformations. The reason for the increase in capacity is because the neighboring parts can distribute the load through the fibers to the unloaded parts

As can be seen in *figure 3.5* and in Suensons test is that not only the fibers directly under the loaded length carry the load but also by neighboring lengths. In an article made by Leijten, Larsen and Van der Put [25] three different approaches to handle the neighboring length (also called effective length) are presented.

The first approach is presented by Madsen et al [11] in year 2000. They proposed that the design code clauses should be based on an effective length, l_{ef}, loaded in uniform compression, corresponding to the ultimate compression strength. Madsen formulated an empirical model which was later modified by Blass and Görlacher [23] according to *equation 3.1*:

$$\frac{F_c}{b\,l_{ef}} = k_c f_{c,90} \tag{3.1}$$

Blass and Görlacher suggested for fully supported load cases: $k_c = 1.25$ for solid wood and $k_c = 1.5$ for glulaminated wood. With fully supported load case means that the support stretches over the total length of a element. l_{ef} is defined in *figure 3.6*. For other discontinuous supports $k_c = 1.0$.
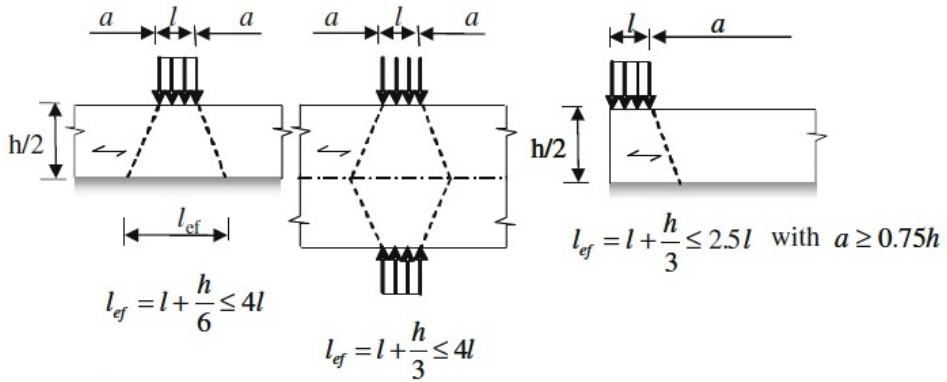
Figure 3.6: The definition of l_{ef} according to Blass and Görlacher [23].

Second model is designed by Riberholt [27] and is based on tests made by Petersen [26] according to *equation 3.2*:

$$f_s = k_c f_{c,90} \tag{3.2}$$

where

$$k_c = (2.38 - \frac{l}{250})\sqrt{\frac{l_{ef}}{l}} \leq 4 \text{ for } n \leq 2.5b$$

The main difference from Madsens equation is that the effective length depends upon the beam height with a stress slope dispersion of 1:3. This is illustrated in *figure 3.7*.
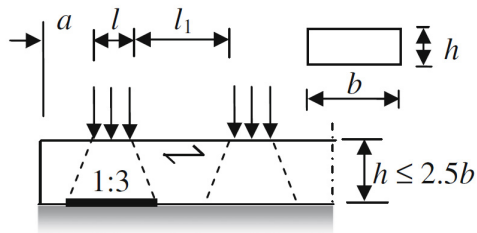
Figure 3.7: Stress dispersion by Riberholt [27].

The third model to handle the effective length is a model formulated by Van der Put. This model is a physical model based on equilibrium method assuming linear-plastic material behavior. The stress field assumed satisfies all boundary conditions with none of the stresses exceeding the plastic failure criterion and is therefore an exact model. For small strains an approximation of 1:1 slope is made and for larger strains 1:1.5, see *figure 3.8*. At large strains the strain hardening is fully developed. Van der Put formulates the bearing capacity as in *equation 3.3*.
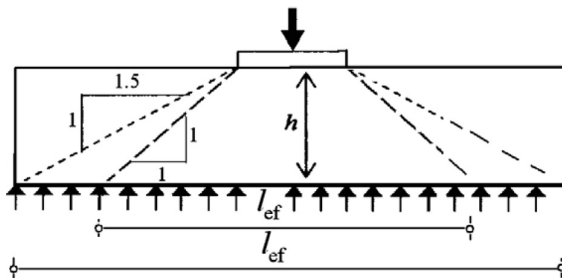
Figure 3.8: Stress dispersion by van der Put [29].

$$\frac{F_c}{bl} = k_{c,90} f_{c,90,d} \tag{3.3}$$

where

$$k_{c,90} = \sqrt{\frac{l_{ef}}{l}} = \sqrt{\frac{l + 3h}{l}}$$

Later in the article the three different methods are compared to test data. A total of 685 test results were evaluated, 576 at 3 % deformation and 109 at 10 % deformation. The models were presented in a normal probability plot and two normal distribution graphs. The later can be seen *figure 3.9* and *figure 3.10*. The conclusion is that Van der Puts physical model is the most accurate and reliable in predicting the effective unloaded length and therefore the bearing strength perpendicular to the grain.
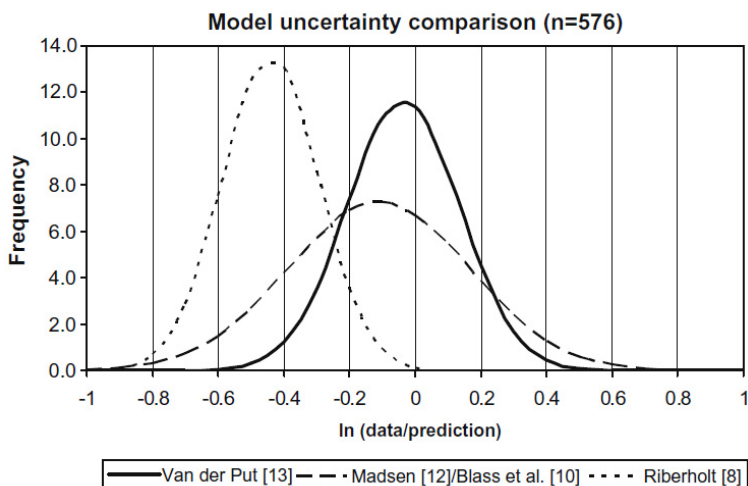
Figure 3.9: Model uncertainty plot at 3 % deformation [25].
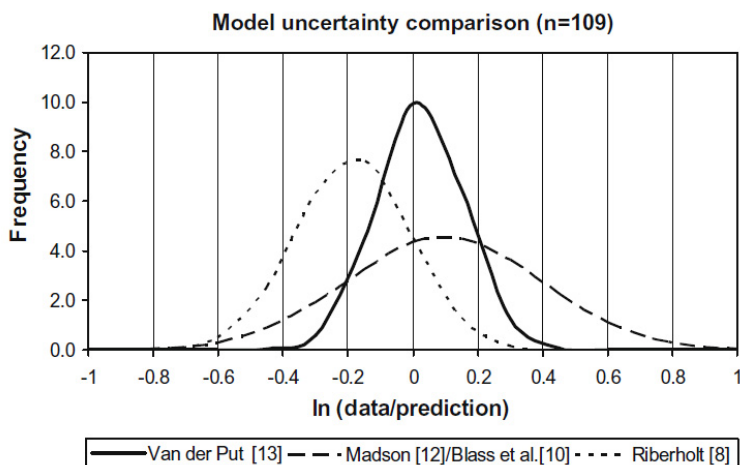
Figure 3.10: Model uncertainty plot at 10 % deformation [25].

In an article made at VTT Technical Research Centre of Finland [12] tests have been made to evaluate the factor $k_{c,90}$ for glulaminated specimen with dimensions 115x1305. Since the support area is a critical design case of large glulam beams, the tests of 600 mm long support lengths were performed. The results points that the average $k_{c,90}$-factor for these tests should be 1.5. An overview over the test results can be seen in *table 3.1*. The conclusion of the performed tests is that $k_{c,90}$ can be taken generally as 1.5 for glulam both in sills and supports without any limitations to the contact length (except length below 400 mm). However, if small deformations adventures the structural system $k_{c,90}$ should be set to 1.25 according

17

to the tests performed. F_{10} is the reaction force when the displacement is 10 mm.

Test specimen	F_{10} kN	σ_{10} N/mm^2	F_{max} kN	δ_{max} mm	σ_{max} N/mm^2	k_{c90} $= \sigma_{max}/f_{c,90}$
1P	235	3.29	318	37	4.47	1.79
1K	266	3.75	318	25	4.49	1.53
2P	251	3.54	324	35	4.58	1.57
2K	265	3.73	324	48	4.57	1.59
3P	282	3.95	311	21	4.36	1.47
3K	267	3.73	311	28	4.35	1.32
4P	265	3.70	300	20	4.20	1.39
4K	257	3.57	300	21	4.18	1.40
mean	261	3.66	314	29	4.40	1.51
var	5.3 %	5.3 %	3.1 %	33.5 %	3.5 %	9.8 %

Table 3.1: Results of the beam tests [12].

3.4 Recommendations in the codes

In modern structural design, there are two criteria to be fulfilled: ultimate and serviceability limit state. Ultimate limit states correspond to failure of the whole structure or part of it and the requirements are quite precise. Serviceability limit states correspond to unacceptable behavior at normal use. One of an unacceptable behavior is for instance large deflections that are visually non-aesthetic. A visual requirement leaves an interval for the designer and the client to decide what is acceptable and not according to any design codes.

Mentioned in previous chapters, there is no brittle failure when the stress exceeds the defined strength value in perpendicular to the grain, $F_{c,90}$, but only large deformations. In an article by Thealandersson and Mårtensson [28] it is proposed that in some loading situations, calculations should be done in serviceability instead of ultimate limit state which is interesting. Taking advantage of a lower partial safety factors wood would be more favorable in meaning of lower stress levels. Ultimately, it would be needed smaller volume of material to withstand the same forces and less expensive designs.

The design capacity perpendicular to the grain is calculated in different ways depending on which code is being used. To illustrate the differences in strength perpendicular to the grain a presentation of the former Swedish code BKR and the new Eurocode 5 is made in ultimate state limit. The explanations are followed by an example for comparing the codes.

3.4.1 Former Swedish code BFS 2010:2 BKR 13

Swedish code treated design of compression perpendicular to the grain according to *equation 3.4* [1]:

$$R_{c,90,d} = k_{c,90} f_{c,90} A \tag{3.4}$$

where

$R_{c,90,d}$ is design value for compression perpendicular to the grain

$f_{c,90,d}$ is design capacity for compression perpendicular to the grain

A is stress loaded area

$k_{c,90}$ is an increase factor which accounts for the unloaded length

The value of $k_{c,90}$ should be put to 1.0 unless the assumptions in following parts applies. If the assumptions applies $k_{c,90}$ could be put at a higher value but maximal 1.75.

For plain timber where $L_1 > 2h$ (L_1 is the contact length and h is the height of the specimen, see *figure 3.11a*) $k_{c,90}$ should be set to:

$k_{c,90} = 1.25$ for massive timber

$k_{c,90} = 1.5$ glulaminated timber

For construction parts on a support, where $L_1 > 2h$, see *figure 3.11b*, $k_{c,90}$ should be set to:

$k_{c,90} = 1.5$ for massive timber

$k_{c,90} = 1.75$ glulaminated timber given that $L < 400$ mm.
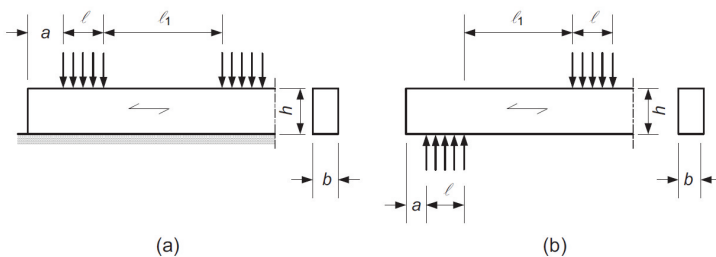
Figure 3.11: Figures in both BKR and Eurocode [4].

3.4.2 Eurocode 5

The following conditions must be fulfilled [4]:

$$\sigma_{c,90,d} < k_c f_{c,90,d} \tag{3.5}$$

with

$$\sigma_{c,90,d} = \frac{F_{c,90,d}}{A_{ef}}$$

where

$\sigma_{c,90,d}$ is design compressive stress in the effective contact area perpendicular to the grain

$F_{c,90,d}$ is design compressive force perpendicular to the grain

$f_{c,90,d}$ is design capacity stress perpendicular to the grain

A_{ef} is the effective contact area

$k_{c,90}$ is factor which handles how the load is applied, the risk for splitting and degree of compression

The effective contact surface at compression perpendicular to the grain, A_{ef}, should be determined regarding the effective contact length parallel to the grain, where the real contact length, L, on each side is increased by 30 mm but not more than a, L or $L_1/2$, see *figure 3.11*.

The value of $k_{c,90}$ should be put to 1.0 unless the assumptions in following parts applies. If the assumptions applies $k_{c,90}$ could be put at a higher value but maximal 1.75.

For plain timber where $L_1 > 2h$ (L is the contact length and h is the height of the specimen, see *figure 3.11a* $k_{c,90}$ should be set to:

$k_{c,90} = 1.25$ for massive timber

$k_{c,90} = 1.5$ glulaminated timber

For construction parts on a support, where $L > 2h$, see *figure 3.11b*, $k_{c,90}$ should be set to:

$k_{c,90} = 1.5$ for massive timber

$k_{c,90} = 1.75$ glulaminated timber given that $L < 400$ mm.

3.4.3 Comparison by an example

Conditions

The geometric conditions that apply are found in *figure 3.12* and *table 3.2*. The glulaminated beam are of class GL32c which equals the former Swedish class L40 (both have the characteristic bending strength f_{mk} 32 MPa). The main difference between the classes is that the strength capacity perpendicular to the grain, f_{c90k}, is 2.7 MPa in Eurocode 5 and 8.0 MPa in BKR.
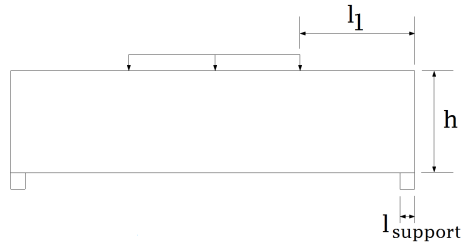
Figure 3.12: Geometry of the setup.

l_1	720	mm
h	630	mm
$l_{support}$	90	mm

Table 3.2: Dimensions for the beam.

Method

The calculations are carried out with equations handled in the previous sub-chapters about the Eurocode and BKR.

Results

$$F_{c90k} = 47 \text{ kN, Eurocode 5}$$
$$F_{c90k} = 83 \text{ kN, BFS 2010:2 BKR 13}$$

Although an effective area is accounted for in Eurocode 5 the drop in characteristic capacity perpendicular to the grain from 8.0 MPa in BKR to 2.7 in Eurocode weights a lot. The characteristic capacity is reduced about to 50 %.

Chapter 4

Reinforced glulaminated beams

This chapter starts with a presentation of reinforced cross sections. The intro is followed by a presentation of Collings model and a method developed in Karlsruhe. Just like in the previous chapter this chapter ends with a calculation example to illustrate the differences between the models. The differences between the former Swedish code BFS 2010:2 BKR 13 and Eurocode 5 are taken into account.

4.1   General introduction
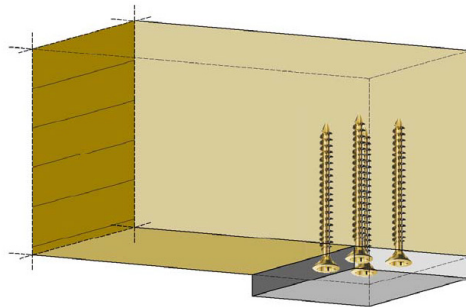
Figure 4.1: Some examples where stress perpendicular to the grain occur [22].

It is of interest to minimize the compressive stresses perpendicular to the grain because, as previously mentioned, the strength perpendicular to the grain is lower than the strength parallel to the grain. An increase of the capacity (in load magnitude) of beam supports could be done by increasing the loaded area or by reinforcing the support area. The reinforcement may be done with self tapping screws or threaded rods made of steel or wood. Francois Collings [24] developed a design method in 2000 which were later evolved in 2006 by Bejtka and Blass. In an article, 'Self-tapping screws as reinforcement in beam supports' [22], three different modes
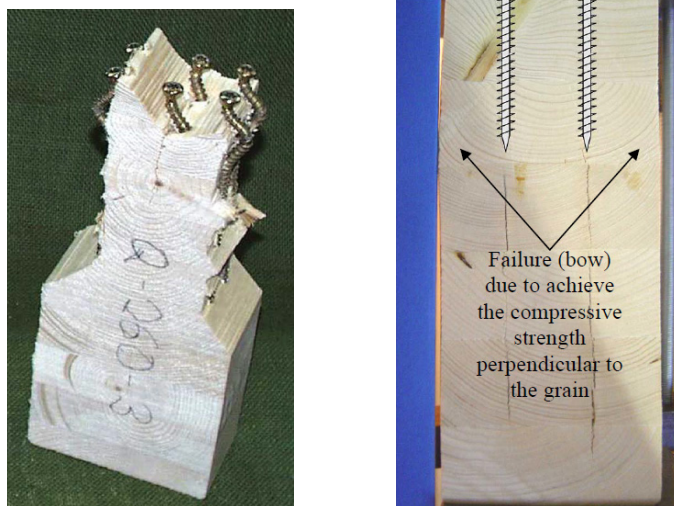
Figure 4.2: To the left, buckling of the screws and to the right, failure in plane formed by the screw tips [22].

of failure are discussed; screws pushing into the timber, buckling of screws and by reaching the compressive strength perpendicular to the grain in the plane formed by the screw tips, see *figure 4.2*.

4.2   Collings method

In 1999-2000 tests were made with reinforcement perpendicular to the grain (with wood reinforcement) by Francois Colling [24]. The tests were performed with different variables such as screw dimensions and closeness, different types of support and timber density. With the results from the tests Colling could derive the following design equation (*equation 4.1*) which simplified says 'Total capacity = load capacity of timber + load capacity of effective scews'.

$$F_{c,90} = f_{c,90}A + k_A n_{ef} F_{D,S} \tag{4.1}$$

where

$F_{c,90}$ is the total capacity of the timber section

$F_{D,S}$ is the load bearing capacity of one screw

k_A is a coefficient depending on the material used for loading
$k_A = 1$ for hard materials such as steel and concrete
$k_A = 0.75$ for softer materials like timber

A is the stress area

n_{ef} $min\{6; \dfrac{b\, l_A}{450\, d_s}\}$

bl_A is the stress area
d_s is the screw diamater

4.3 Method developed in Karlsruhe

As said in general description, this model is evolved from Collings method and by means of new and more tests this model can more accurately consider the effect of screws as reinforcement according to Formolo and Granström [6]. This model is developed considering three different types of failure modes which each will be shortly explained below. The article [22] also contains how calculate the effective stiffness perpendicular to the grain at a reinforced beam support but only for direct loading situations and will not be handled in this thesis.

4.3.1 Pushing in capacity

The first mode of failure is when a screw is pushed into the timber. According to the tests the pushing-in capacity is equal to the withdrawal capacity, $F_{ax,Rk}$, see *equation 4.2* for BFS 2010:2 BKR 13 and *equation 4.3* for Eurocode 5 respectivly.

$$F_{ax,k,Rk} = 11(2.5 + d)(l_g - d) \tag{4.2}$$

where

d the screws diameter (mm)
l_g the threaded anchoring length (mm)

$$F_{ax,k,Rk} = \frac{n_{ef}\, f_{ax,k}\, d\, l_{ef}\, k_d}{1.2\, cos^2\alpha + sin^2\alpha} \tag{4.3}$$

where

$$f_{ax,k} = 0.52\, d^{-0.5}\, l_{ef}^{-0.1}\, \rho_k^{0.8}$$
$$k_d = min \left\{ \begin{array}{c} \frac{d}{8} \\ 1 \end{array} \right\}$$

25

$F_{ax,Rk}$ is is the characteristic withdrawal strength perpendicular to the grain

n_{ef} is the effective number of screws

l_{ef} is penetration deep

ρ_k is the characteristic density in kg/m^3

α is the angle between the screw axis and the grain direction

4.3.2   Buckling of screws

The second mode of failure is buckling of a screw. The reinforcing screws are axially loaded in compression. The buckling load for axially loaded screws, which are embedded in timber, is determined by a numerical model, see *figure 4.3*.
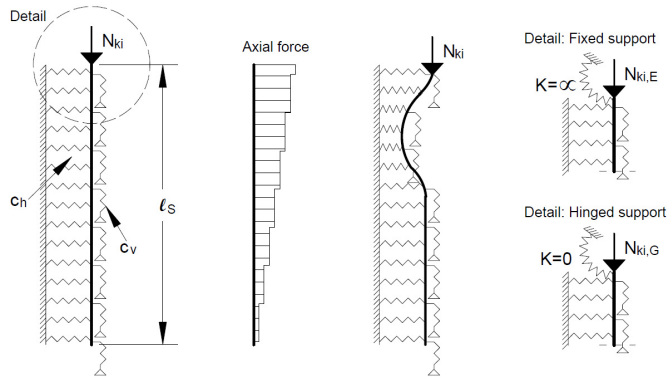
Figure 4.3: The numerical model used to calculate the buckling load [22].

The best correlation between the test results and the calculated values can be achieved with elastic foundation-stiffness c_h, see *equation 4.4* and c_v, see *equation 4.5*.

$$c_h = \frac{(0.22 + 0.014d)\rho}{1.17 \, \sin^2(\alpha) + \cos^2(\alpha)} \tag{4.4}$$

$$c_v = 2.34 \, \frac{(\rho \, d)^{0.2}}{(l_s)^{0.6}} \tag{4.5}$$

Whether a fixed support or a hinged support should be assumed, a hinged support must be assumed. A fixed support, i.e. a clamped screw head, may only be assumed by clamping the screw heads in the steel plate. For this, it is necessary to countersink the steel plate in the form of the screw heads in such a way as the surface of the screw heads is flush with the lower steel plate surface. The buckling load was calculated in a finite element program for several different test setups.

For long and slender beams the buckling load can be calculated with N_{kik}, see *equation 4.6* for beam without supports and *equation 4.7* for beam with two supports. Worth noticing is that the equations for buckling load are independent of the screw length.

$$N_{kik} = \sqrt{c_h \, E_s \, I_s} \tag{4.6}$$

$$N_{kik} = 2 \, \sqrt{c_h \, E_s \, I_s} \tag{4.7}$$

where $E_s = 210$ GPa and $I_s = \frac{\pi}{64}(0.7 \, d)^4$.

4.3.3 Load distribution in beam supports

The third and last mode of failure is characterized by reaching the compressive strength perpendicular to the grain in a plane formed by the screw tips. The length of the plane is calculated differently depending on loading situation. In the article two different beam supports were studied with directly loaded sleepers and indirectly loaded beam supports. The different test setups can be seen in *figure 4.4* and *figure 4.5*.
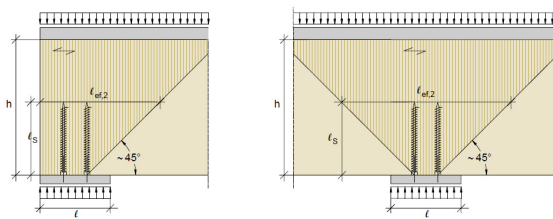
Figure 4.4: Load distribution in directly loaded supports [22].
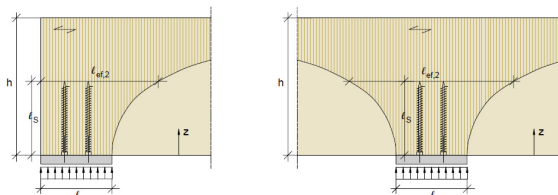
Figure 4.5: Load distribution in indirectly loaded supports [22].

The length of the planes in the directly loaded case is linear can be calculated with interpolation but in the indirectly case *equation 4.8* (single load distribution) and *equation 4.9* (double-sided load distribution).

$$l_{ef,2} = l + 0.25 \, l_s \, e^{\frac{3.3 \, l_s}{h}} \tag{4.8}$$

$$l_{ef,2} = l + 0.58 \, l_s \, e^{\frac{3.6 \, l_s}{h}} \tag{4.9}$$

4.3.4   Design model

The three different failure modes above end up in the following design method. A reinforced beam support may be calculated with *equation 4.10*:

$$R_{90,d} = min \left\{ \begin{array}{l} nR_d + k_{c,90}l_{ef}b\,f_{c,90,d} \\ bl_{ef,2}f_{c,90,d} \end{array} \right\} \tag{4.10}$$

where

$$R_d = min \left\{ \begin{array}{l} R_{ax} \\ R_{c,d} \end{array} \right\}$$

$$R_{c,d} = \kappa_c\,N_{pl}$$

$$\kappa_c = 1 \text{ for } \bar{\lambda} \leq 0.2$$

$$\kappa_c = \frac{1}{k + \sqrt{k^2 - \bar{\lambda}^2}} \text{ for } \bar{\lambda} > 0.2$$

$$k = 0.5[1 + 0.49(\bar{\lambda} - 0.2) + \bar{\lambda}^2]$$

$$\bar{\lambda} = \sqrt{\frac{N_{pl,d}}{N_{ki,d}}}$$

and

$F_{ax,d}$ is design value of the withdrawal capacity, see 'Pushing in capacity' above

n is is the number of screws

b is the width of the beam

l_{ef} $l_{ef} = l + min\,[l; 30\,\mathrm{mm}]$ for single-sided load distribution
$l_{ef} = l + 2\,min\,[l; 30\,\mathrm{mm}]$ for double-sided load distribution

$l_{ef,2}$ see *figure 4.4* and *figure 4.5*

$k_{c,90}$ coefficient $k_{c,90} \in [1; 1.75]$ for the load distribution, see chapter 3

$f_{c,90,d}$ design value of the compressive strength perpendicular to the grain

$N_{pl,d}$ design value of the plastic load-carrying capacity calculated with the cross section of the core diameter of the screw

$N_{ki,d}$ design value of the buckling load for a screw taking into account the elastic foundation, for details see sub-chapter 'Buckling of screws'

4.4   Adhesive joints

The art of bonding is very old, about 4000 years before Christ, and the bonding between the wood components began in the Egyptian Faron materials manufacturing. But it was not until the 1900s, with the help of scientific studies, the chemical and physical properties were explored. Without going to deep into chemistry, the mechanical bonds with glue between different materials are depending on the molecules electrical attraction to each other. When the glue is in fluid form the movable molecules in the glue can orient themselves and bond with each wood part. This leads to a mechanical bonding between the parts with glue between the parts [17].

There are different glues for different materials, purposes and environments. For instance epoxy glue hardens quickly and with minimal shrinkage and is therefore favorable when completely sealing is required. Other benefits of epoxy, it is widely available to tailor the properties to the conditions that apply. There are slow and fluid. There are adhesives with short and long hardening times. The disadvantage of this glue is that it is expensive compared to other adhesives. Examples of applications include bonding of metal, plastic and rubber to wood [17]. In this thesis, the glue is used for bonding between the reinforcement and the beam.

4.5   Comparing Colling and Karlsruhe model with BFS 2010:2 BKR 13 and Eurocode 5

The calculation in this comparison will be done with five different support lengths to see if there is any connection in the stress capacity depending on the support length. The results will later be compared with the FE-models.

4.5.1   Conditions

In the following calculation the beam capacity compression perpendicular to the grain with reinforcement will be calculated. There are two setups, one with wooden dowels f_{yk} 60 MPa and one with countersunk screws of model M12 with f_{yk} 400 MPa will be used. All values are characteristic values. The interaction between the wood in the beam and the screws are modeled by glue. However, the stiffness properties of glue are neglected because its complexity and due to the layer is very thin and consequently having little effect on the results. The geometrical conditions that apply for the beams and screws can be found in *figure 4.6* and in *table 4.1*. The material properties are found in *table 4.2*, *table 4.3* and *table 4.4*.
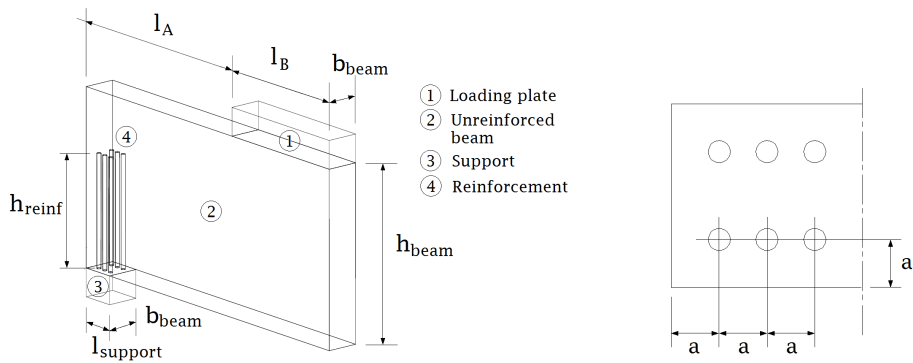
Figure 4.6: Geometry of the beam. This figure shows a conceptual view when the support length is 120 mm. The dimensions for each length can be found in *table 4.1*.

$l_{support}$	**60**	**90**	**120**	**150**	**180**	mm
l_A	690	720	750	780	810	mm
l_B	560	530	500	470	440	mm
h_{beam}	630	630	630	630	630	mm
b_{beam}	115	115	115	115	115	mm
a	30	30	30	30	30	mm

Table 4.1: Table over geometry for each support length.

ρ	450	kg/m^3
$k_{c,90}$	1	
$f_{c,90,k}$ [BKR 13]	8	MPa
$f_{c,90,k}$ [EC5]	2.7	MPa
c_h	149	N/mm^2

Table 4.2: Material properties of wood.

L_{screw}	400	mm
d_{screw}	19	mm
$d_{screw,nom}$	17	mm
f_{yk}	60	MPa

Table 4.3: Geometry and materials properties of wooden dowels.

L_{screw}	400	mm
d_{screw}	12	mm
$d_{screw,nom}$	10.3	mm
f_{yk}	400	MPa

Table 4.4: Geometry and materials properties of threaded steel screws.

4.5.2 Method

The beam is only interesting at the support therefore only half of the beam is drawn. All calculations have been carried out with equations from the building codes stated in previous sub chapter. For details, see *Appendix 12.1* and *Appendix 12.2*.

4.5.3 Results

The results are plotted with different support lengths and the total capacity for the cross section, see *figure 4.7 - 4.10*. Collings design method is clearly more conservative compared to to the method developed in Karlsruhe. It is also clear that the higher characteristic value in BKR have a big influence for the total capacity for a reinforced cross-section perpendicular to the grain.
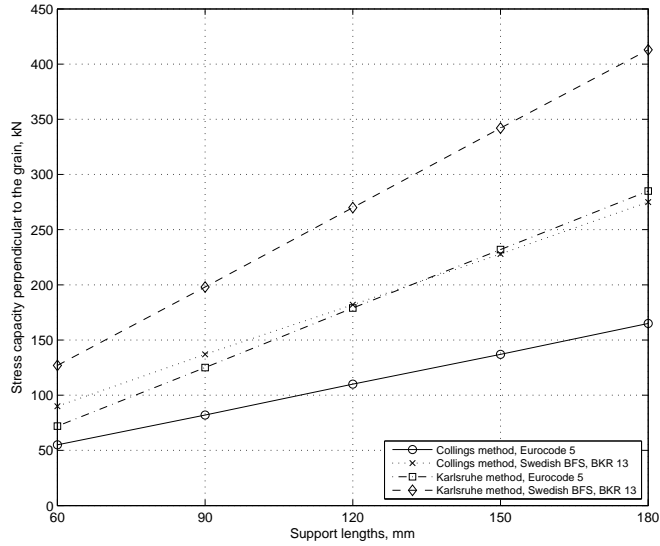
Figure 4.7: Capacity (force magnitude) of reinforced beam (dowels) with different support lengths.
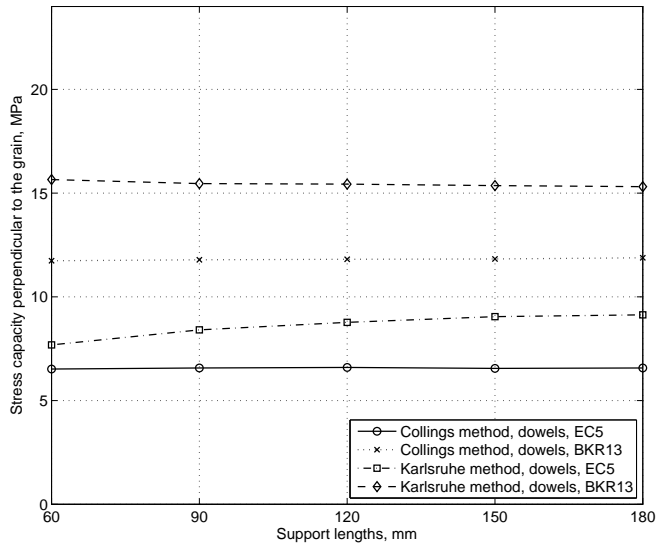
Figure 4.8: Capacity (stress level) of reinforced beam (dowels) with different support lengths.
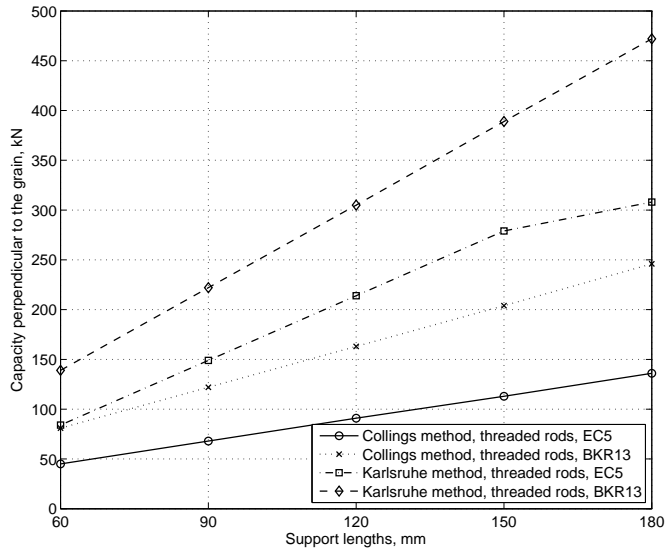
Figure 4.9: Capacity (force magnitude) of reinforced beam (threaded rods) with different support lengths.
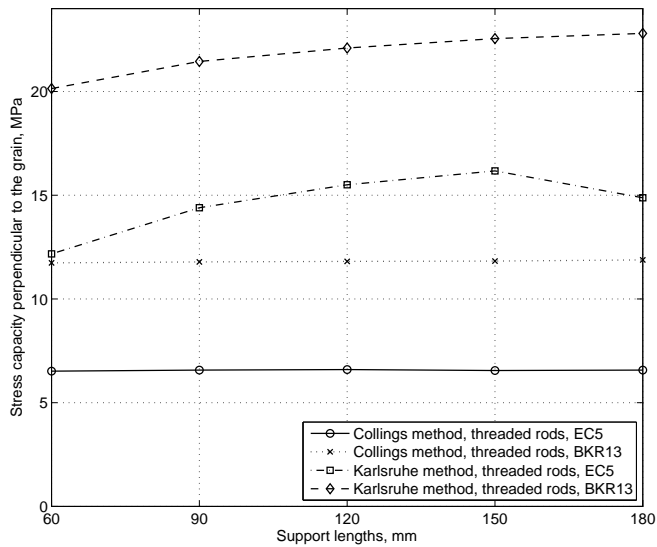
Figure 4.10: Capacity (stress level) of reinforced beam (threaded rods) with different support lengths.

Chapter 5

Laboratory tests

Parallel to this thesis study another Master's thesis study handling strength perpendicular to the grain have been worked out by Daniel Edh and Fredrik Hasselqvist at the Division of Structural Engineering. The objective of their thesis is similar but by means of laboratory testings. This is advantageous due to it is possible to compare the finite element models and judge the creditability of the models. This chapter gives an overview of the tests and results which are interesting for comparison with the FE-models. For details the reader is referred to their thesis [5]. In the end of this chapter a calculation of the foundation stiffness are done to compare with the results from chapter 4.

5.1 Conditions

A total of 40 beams were tested with different setups. The setups were $90x270$, $90x360$, $90x630$ with nail plates, $115x630$ unreinforced and $115x630$ with reinforcement in form of wooden dowels or threaded steel screws. The length varied between the setups (1.6 m and 2.5 m) but the support lengths were the same for all setups; 60, 90 and 120 mm. The average density of the beams were 460 kg/m^3. The wooden dowels were in flush with the beams bottom but the threaded steel screws were not. They were irregular pushed in 2-8 mm which is shown in *figure 5.1*.

5.2 Procedure

The beams were exposed to load until the maximal capacity was reached. This could be done by observing graphs seeing when there is not any increase in load but only in deformation. With the reinforcing beams the maximal load was given when a dowel or screw buckles. The devices for measuring the deformation at the supports is shown in *figure 5.2*. There were two measure devices at each support

Figure 5.1: The threaded steel screws were irregularity pushed in [5].

and a mean value was used. The load magnitude was measured form a sensor in the loading machine.

5.3 Results

The results of importance to compare with the finite element models are the unreinforced beams and the beams reinforced with wooden dowels and threaded steel screws. The laboratory results of these setups are shown as images followed by stress-deformation plots with different support lengths.

Figure 5.2: To the left, the setup and to the right, a unreinforced beam cracks at the bottom right side of the beam [5].

Figure 5.3: To the left, a reinforced beam with dowels cracks both at the right and left side of the beam. To the right, a view from the bottom side of the beam [5].

Figure 5.4: To the left, a reinforced beam with threaded steel rods cracks. To the right, a view from the bottom side of the beam [5].
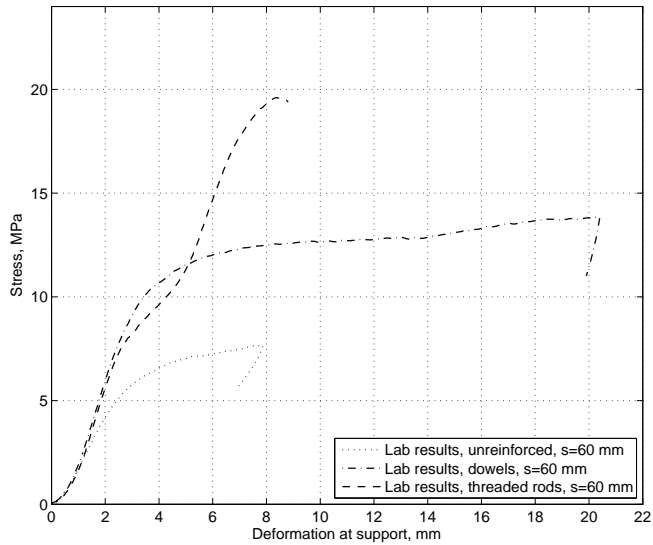
Figure 5.5: Stress-deformation plot over mean values, support length 60 mm (2 dowels/rods).
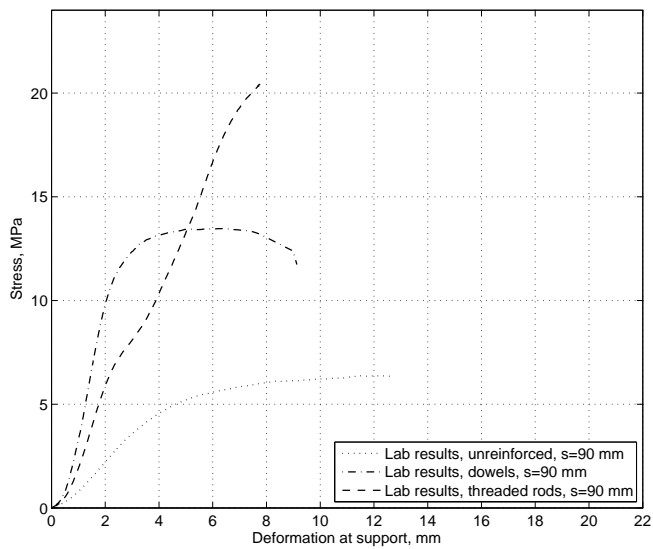
Figure 5.6: Stress-deformation plot over mean values, support length 90 mm (4 dowels/rods).
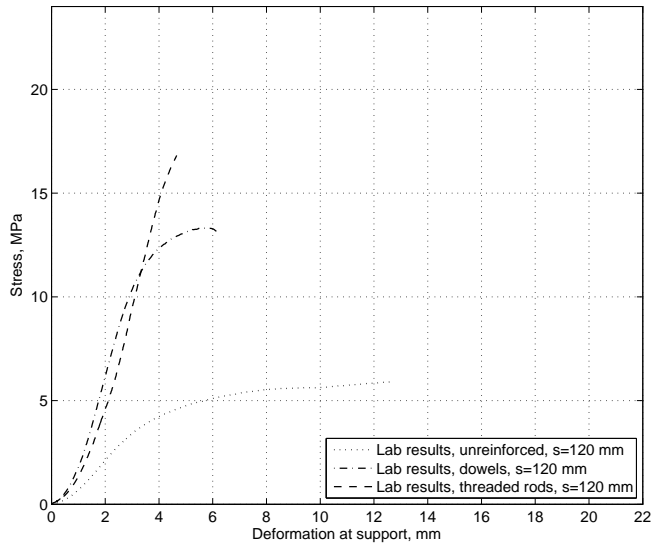
Figure 5.7: Stress-deformation plot over mean values, support length 120 mm (6 dowels/rods).

5.4 Calculating the elastic foundation stiffness

It is of interest to find the stiffness foundation in the laboratory test and compare the results with the values from chapter 4 calculated by equations in the article by Betjka and Blass [22].

5.4.1 Method
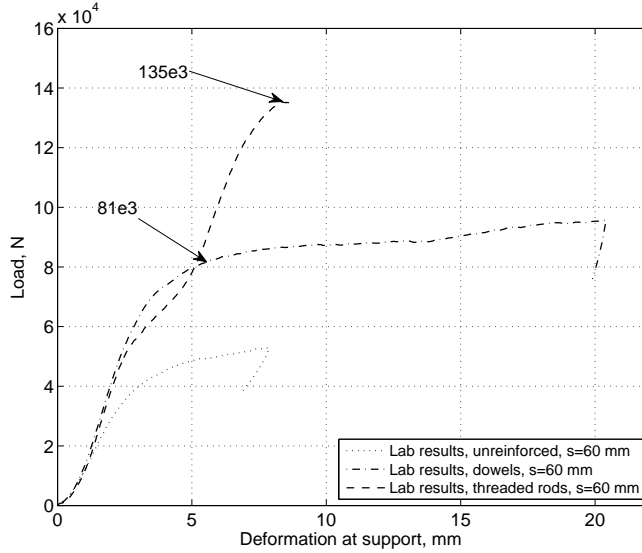
Figure 5.8: Mean values from the laboratory tests with support length 60 mm. The arrowheads points out where the elastic behavior goes into plastic for the wooden dowels and the threaded steel screws.

The stiffness can be found by manipulating *equation 5.1* to *equation 5.2*. P_{cr} is read from *figure 5.8*, $E = 210\,GPa$ and $I = \frac{\pi}{64}(d_{nom})^4$. Worth noticing is that the value shown in the figure is for one pair of reinforcement so the value must be divided by two.

$$P_{cr} = \sqrt{k\,E_s\,I_s} \tag{5.1}$$

$$\Longleftrightarrow$$

$$k = \frac{(P_{cr})^2}{E_s\,I_s} \tag{5.2}$$

5.4.2 Results

With previous stated equation the horizontal stiffness foundation, k, is 39 N/mm^2 for the wooden dowels and 30 N/mm^2 for the threaded rods made by steel. The values are alike which is reasonable due to the beam is working as the horizontal stiffness layer. According to the equations in chapter 4 the diameter should have an effect which is also shown by a difference of 30 %. When comparing the horizontal stiffness values with the values theoretical calculated in chapter 4, the stiffness foundation for corresponding setup is 176 N/mm^2 for the wooden dowels, which is about five times larger. Corresponding stiffness foundation for threaded rods is 140 N/mm^2 which is also about five times larger. The conclusion is that the model developed in Karlsruhe cannot capture the horizontal stiffness foundation when calculating with pre-drilled threaded reinforcement.

Chapter 6

The Finite element method and ABAQUS

The Finite element method have been used for all strain and stress calculations in this thesis. This chapter starts with a short introduction to the Finite element method and basic differential equation the method is build up on. The chapter ends with a presentation of the commercial program ABAQUS.

6.1   The Finite element method

All the physical phenomena encountered in engineering mechanics are modeled by differential equations, and usually the problem addressed is too complicated to be solved by classical analytical methods [13]. The Finite element method was found in the 1960s and is a numerical approach by which general differential equations can be solved in an approximate manner. The differential equations describes a certain region which can be one-, two or three dimensional. What characterizes FEM is that a body which should be analyzed is divided into smaller parts, so called finite elements. Over these part-areas relatively simple approximations can be made which corresponds with reality even if the full-size body behaves very non linear. The corners in each element are called nodal point (or nodes) and the nodes together form a finite element mesh. The choice of element mesh is important to get a result that matches the actual behavior in reality.

Since it is often tens of thousands of unknown degrees of freedom, the system of equations cannot be solved without computer calculations. A finer mesh, and therefore an increased amount of (Degree of freedoms) DOFs, will normally generate a more accurate solution. It is often favorable to intensify the mesh where high gradients occurs. This leads however to increased time of calculation.
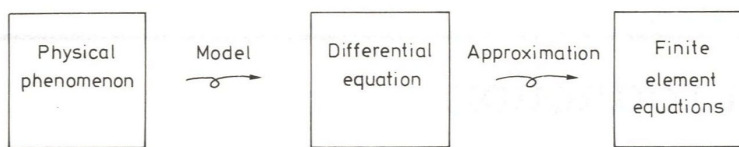
Figure 6.1: Steps in engineering mechanics analysis [13].

6.1.1 Weak form of equilibrium equations (three dimensional case)

For three dimensional problems the differential equations of equilibrium are given by:

$$\tilde{\nabla}^T \boldsymbol{\sigma} + \mathbf{b} = \mathbf{0} \tag{6.1}$$

where

$$\tilde{\nabla}^T = \begin{bmatrix} \frac{\partial}{\partial x} & 0 & 0 & \frac{\partial}{\partial y} & \frac{\partial}{\partial z} & 0 \\ 0 & \frac{\partial}{\partial y} & 0 & \frac{\partial}{\partial x} & 0 & \frac{\partial}{\partial z} \\ 0 & 0 & \frac{\partial}{\partial z} & 0 & \frac{\partial}{\partial x} & \frac{\partial}{\partial y} \end{bmatrix} \quad \boldsymbol{\sigma} = \begin{bmatrix} \sigma_{xx} \\ \sigma_{yy} \\ \sigma_{zz} \\ \sigma_{xy} \\ \sigma_{yz} \end{bmatrix} \quad \mathbf{b} = \begin{bmatrix} b_x \\ b_y \\ b_z \end{bmatrix} \tag{6.2}$$

By carrying out the matrix multiplication of *equation 5.1* gives:

$$\frac{\partial \sigma_{xx}}{\partial x} + \frac{\partial \sigma_{xy}}{\partial y} + \frac{\partial \sigma_{xz}}{\partial z} + b_x = 0$$

$$\frac{\partial \sigma_{yx}}{\partial x} + \frac{\partial \sigma_{yy}}{\partial y} + \frac{\partial \sigma_{yz}}{\partial z} + b_y = 0 \tag{6.3}$$

$$\frac{\partial \sigma_{zx}}{\partial x} + \frac{\partial \sigma_{zy}}{\partial y} + \frac{\partial \sigma_{zz}}{\partial z} + b_z = 0$$

where the traction vector t must fulfill the boundary conditions:

$$\mathbf{t} = \begin{bmatrix} t_x \\ t_y \\ t_z \end{bmatrix} \qquad \begin{aligned} t_x &= \sigma_{xx} n_x + \sigma_{xy} n_y + \sigma_{xz} n_z \\ t_y &= \sigma_{yx} n_x + \sigma_{yy} n_y + \sigma_{yz} n_z \\ t_z &= \sigma_{zx} n_x + \sigma_{zy} n_y + \sigma_{zz} n_z \end{aligned} \tag{6.4}$$

The objective is to determine the weak form of the differential equations of equilibrium. By using the Green-Gaus theorem it is possible to integrate the equilibrium equation and derive the weak form:

$$\int_V (\tilde{\nabla} \mathbf{v})^T \sigma dV = \int_S \mathbf{v}^T \mathbf{t} dS + \int_V \mathbf{v}^T \mathbf{b} dV \tag{6.5}$$

where v is an arbitrary vector which weighs the numerical errors.

$$\mathbf{v} = \begin{bmatrix} v_x \\ v_y \\ v_z \end{bmatrix} \tag{6.6}$$

6.1.2 FE formulation of three-dimensional elasticity

With the weak form (*equation 6.5*) of the equilibrium equations it is straightforward to derive the FE equations for three-dimensional elasticity. By approximating the vector $\mathbf{u}$ with

$$\mathbf{u} = \mathbf{Na} \tag{6.7}$$

where $\mathbf{N}$ is the global matrix of shape functions and $\mathbf{a}$ contains the local displacements. The Galerkin method means that the weight vector $\mathbf{v}$ is chosen in accordance with

$$\mathbf{v=Nc} \tag{6.8}$$

As $\mathbf{v}$ and $\mathbf{c}$-matrix are arbitrary it follows that *equation 6.4* can be rewritten as:

$$\tilde{\nabla}\mathbf{v=Bc} \quad where \quad \mathbf{B} = \tilde{\nabla}\mathbf{N} \tag{6.9}$$

Putting together *equation 6.8* and *equation 6.9* into the weak formulation, *equation 6.5*, it leads to:

$$\int_V \mathbf{B}^T \sigma dV = \int_S \mathbf{N}^T \mathbf{t}dS + \int_V \mathbf{N}^T \mathbf{b}dV \tag{6.10}$$

When the global matrix of shape functions $\mathbf{N}$ has the dimension $3 \times 3n$ where n is the number of nodal points in the entire body, and as $\mathbf{b}$ has the dimension 3×1, $\mathbf{N}^T \mathbf{b}$ has the dimension $3n \times 1$. The right hand side of *equation 6.10* can be viewed as forces acting at the nodal points.

Introducing the constitutive model and assuming the material responds elastic $\boldsymbol{\sigma}$ can be written as

$$\boldsymbol{\sigma} = \mathbf{D}\boldsymbol{\epsilon} - \mathbf{D}\boldsymbol{\epsilon}_0 \tag{6.11}$$

By putting together *equation 6.7*, *equation 6.9* in *equation 6.11* it can be written as

$$\boldsymbol{\sigma} = \mathbf{DBa} - \mathbf{D}\boldsymbol{\epsilon}_0 \tag{6.12}$$

With *equation 6.12 equation 6.10* takes the form

$$\left(\int_V \mathbf{B}^T \mathbf{DB}dV\right)\mathbf{a} = \int_S \mathbf{N}^T \mathbf{h}dS + \int_V \mathbf{N}^T \mathbf{t}dV + \int_V \mathbf{B}^T \mathbf{D}\boldsymbol{\epsilon}_0 dV \tag{6.13}$$

Introduce boundary conditions which are expressed either in terms of a prescribed traction vector $\mathbf{t}$, the *natural boundary condition*, or a prescribed displacement vector $\mathbf{u}$, the *essential boundary condition*. By rewriting the boundary conditions they become $\mathbf{h}$ and $\mathbf{g}$, see *equation 6.14* and *equation 6.15* respectively.

$$\mathbf{t} = \mathbf{Sn} = \mathbf{h} \tag{6.14}$$

$$\mathbf{u} = \mathbf{g} \tag{6.15}$$

The traction vector $\mathbf{t}$ is known along the boundary S_h and the displacement vector $\mathbf{u}$ is known along the border S_g. The sought FE-formulation can finally be written as.

$$\left(\int_V \mathbf{B}^T \mathbf{D} \mathbf{B} dV \right) \mathbf{a} = \int_{S_h} \mathbf{N}^T \mathbf{h} dS + \int_{S_g} \mathbf{N}^T \mathbf{t} dS + \int_V \mathbf{N}^T \mathbf{b} dV + \int_V \mathbf{B}^T \mathbf{D} \epsilon_0 dV \tag{6.16}$$

In order to write the formulation in compact fashion, the following matrices are defined:

$$\mathbf{K} = \int_V \mathbf{B}^T \mathbf{D} \mathbf{B} dV \tag{6.17}$$

$$\mathbf{f_b} = \int_{S_h} \mathbf{N}^T \mathbf{h} dS + \int_{S_g} \mathbf{N}^T \mathbf{t} dS \tag{6.18}$$

$$\mathbf{f_l} = \int_V \mathbf{N}^T \mathbf{b} dV \tag{6.19}$$

$$\mathbf{f_o} = \int_V \mathbf{B}^T \mathbf{D} \epsilon_0 dV \tag{6.20}$$

Where $\mathbf{K}$ is the stiffness matrix, $\mathbf{f_b}$ the boundary vector, $\mathbf{f_l}$ the load vector and $\mathbf{f_0}$ is the initial strain vector. *Equation 6.16* can be written as:

$$\mathbf{K}\mathbf{a} = \mathbf{f_b} + \mathbf{f_l} + \mathbf{f_o} \tag{6.21}$$

and by defining the load vector as the sum of all force vectors on the right side *equation 6.21* can be written in standard FE formulation:

$$\mathbf{K}\mathbf{a}{=}\mathbf{f} \tag{6.22}$$

6.1.3   Isoparametric finite elements

Normally, the sides of a quadrilateral and brick elements must be parallel to the coordinate axes in order to behave in a compatible manner. This restriction is very difficult to fulfill when modeling bodies with arbitrary geometries. However, it can be done by using isoparametric elements [13].

When modeling bodies with arbitrary geometries the finite elements must be allowed to have curved boundaries, i.e. general shapes. Consider a cubic region in a local $\xi\eta\zeta$-coordinate system that is bound by $\xi{\pm}1$, $\eta{\pm}1$ and $\zeta{\pm}1$. The local region is called the parent domain. This simple geometric shape in the local coordinate system is mapped, transformed, into more a more complex geometry in the global Cartesian-xyz-coordinate system. The global region is called global domain, see *figure 6.2*.
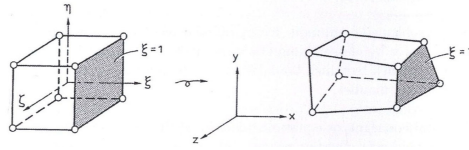
Figure 6.2: Eight-node three-dimensional isoparametric element [13].

For every point in the $\xi\eta\zeta$-coordinate system there is a corresponding point in the xyz-coordinate system. The mapping is therefore done described by

$$x = x(\xi, \eta, \zeta) \quad y = y(\xi, \eta, \zeta) \quad z = z(\xi, \eta, \zeta) \tag{6.23}$$

Differentiating *equation 6.23* and using the chain rule of partial differentiation, it leads to an expression which allows the transformation between the two domains, see *equation 6.24*.

$$\begin{bmatrix} dx \\ dy \\ dz \end{bmatrix} = \begin{bmatrix} \frac{\partial x}{\partial \xi} & \frac{\partial x}{\partial \eta} & \frac{\partial x}{\partial \zeta} \\ \frac{\partial y}{\partial \xi} & \frac{\partial y}{\partial \eta} & \frac{\partial y}{\partial \zeta} \\ \frac{\partial z}{\partial \xi} & \frac{\partial z}{\partial \eta} & \frac{\partial z}{\partial \zeta} \end{bmatrix} \begin{bmatrix} d\xi \\ d\eta \\ d\zeta \end{bmatrix} \tag{6.24}$$

The Jacobian matrix $\mathbf{J}$ related to the mapping in *equation 6.24*, is defined by

$$\mathbf{J} = \begin{bmatrix} \frac{\partial x}{\partial \xi} & \frac{\partial x}{\partial \eta} & \frac{\partial x}{\partial \zeta} \\ \frac{\partial y}{\partial \xi} & \frac{\partial y}{\partial \eta} & \frac{\partial y}{\partial \zeta} \\ \frac{\partial z}{\partial \xi} & \frac{\partial z}{\partial \eta} & \frac{\partial z}{\partial \zeta} \end{bmatrix} \tag{6.25}$$

If the values in the parental domain are the ones to be determined given dx and dy, it follows that

$$\begin{bmatrix} dx \\ dy \\ dz \end{bmatrix} = \mathbf{J}^{-1} \begin{bmatrix} d\xi \\ d\eta \\ d\zeta \end{bmatrix} \tag{6.26}$$

To fulfill the convergence requirement the compatibility and the completeness requirement must be satisfied. If an element behaves in a conforming way, i.e. compatible manner in the parent domain, its isoparametric version also behaves conforming and the adjacent elements will match appropriately. The completeness requirement is satisfied if the sum of all values of the element shape function in every node in the element is equal to 1, see *equation 6.27*.

$$\sum_{i=1}^{n} N_i^e = 1 \tag{6.27}$$

6.2 ABAQUS

FEM is a general method for calculations but the solutions are often complex and therefore it is favorable using finite element program for modeling. In this thesis ABAQUS/CAE 6.10-2 is used for modeling. ABAQUS is a general program in which both static and dynamic calculations can be done. Analysis can be done in both two- and three dimensions from airplanes and skyscrapers to screws and cell buckling at microscopic perspective [19]. To transact a calculation there are different modules which helps the user for instance to create the geometry and boundary conditions. The modules are described below:

- *Part module*: In the part module the geometry for each part is created. A model consists often of more than one part. It is possible to model in 3D, 2D Planar and axisymmetric. In the part module the type of element is chosen, solid, shell or membrane for which is being used in calculations.

- *Property module*: Material- and section properties are assigned. ABAQUS handles many different material models for mechanical calculations, both elastic and plastic. Properties used in this thesis is for instance isotropic elastic behavior, Youngs modulus and Poissons ratio.

- *Assembly*: In this module all parts are assembled and placed geometrically where they belong.

- *Step*: In the step-module it is possible to define which calculation to be carried out. In this module it is defined wether the calculations should be done in a static or dynamic way.

- *Interactions*: If and how a part interacts with another part it is defined in this module. A common interaction is friction which can be described in many ways, for instance in tangential and normal direction.

- *Load*: Loads and boundary conditions are set. Example of loads are concentrated forces and distributed loads. A boundary condition can be rigid or a specified displacement.

- *Mesh*: This is where the finite element mesh is created. In ABAQUS there are several different element shapes to choose from, like cubes or tetrahedrons. Meshing technique and what kind type of element is also decided in this module.

- *Job*: The job is created, written in an input file and sent to the solver.

- *Visualization*: In the final module it is possible to analyze the calculation with the chosen outputs.

Chapter 7

The models for unreinforced wood

In this chapter the unreinforced beams are modeled. The assumptions and limitations of the Finite element models are presented and followed by the geometries for each model. Material, mesh, boundary conditions and interactions are presented. The results are compared with the lab tests to verify the models creditability and the effect of different support lengths can be observed. The unreinforced beams are compared with the reinforced beams in chapter 8. Chapter 7 ends with a proposal of the increase factor, $k_{c,90}$, depending on variables such as allowable deformation and support length.

7.1 Assumptions and limitations of the FE-model

All materials have a variability or variation in properties. This is especially true for wood, as this material grows in the nature and is not manufactured in a factory. In reality wood is a highly inhomogeneous and every beam differs from each other in material properties due to reasons mentioned in chapter 2. Even if glue-laminated timber is considered, with the effect of lamellas, there are still variables in the model that have to be neglected in order to make the model simple and efficient.

The glue-laminated beams are modeled as one part which neglects the different layers of lamellas. The assumption is based on every lamella is assumed to share the same material properties.

The load in the model was applied as a prescribed displacement instead of an applied force. The displacement (which simulates the load) is set in vertical negative y-direction. This method is called displacement control and has several benefits compared to load control. One of the benefits is that the displacement control simulates the behavior in the laboratory tests. Another benefit concerns the increase

of probability of getting convergence during numerical analysis [20], see *figure 7.1*.
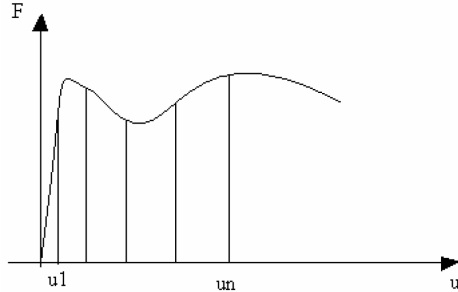
Figure 7.1: Displacement controlled loading [6].

In real time it is a dynamic situation but the leadtime is very slow and therefore the time-dependent matrices $\ddot{u}$ and $\dot{u}$ in the dynamic equation, *equation 7.1*, are almost zero. Therefore the calculations will be done as a static step, see *equation 7.2*.

$$M\ddot{u} + C\dot{u} + Ku = f \tag{7.1}$$

$$Ku = f \tag{7.2}$$

7.2 Geometry

Due to symmetry only half of the beams will be modeled, see *figure 7.2*. This assumption leads to the number of elements can be reduced by 50 % and therefore reduces the time for every new calculation. The unreinforced beams consits of two different cross-sections, $90x270$ and $115x630$. The length of the beams is 2.5 m. The distance from the beam end to the loading plate, l_A, depends on the support length and the height of the beam according to *equation 7.3*. An overview over the different dimensions l_A and l_B can be seen in *table 7.1*.
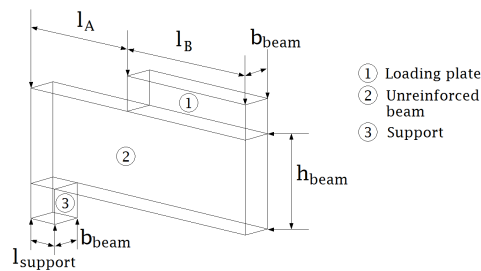
Figure 7.2: Geometry of the unreinforced beams. The thickness of the loading plate and the support is the same as the beam thickness (90 and 115 mm).

$$l_A = h_{beam} + l_{support} \qquad\qquad (7.3)$$

$\mathbf{l_{support}}[\mathrm{mm}]$	$\mathbf{l_A}[\mathrm{mm}]$	$\mathbf{l_B}[\mathrm{mm}]$
60	690	560
90	720	530
120	750	500

Table 7.1: Dimensions depending on different support lengths.

7.3 Materials

The support and the simulated loading plate are made of steel with properties as in *table 7.2* below.

Parameter	Value
E, GPa	210 GPa
ν	0.3

Table 7.2: Properties of steel.

In ABAQUS there is no standard model for handling woods behavior when the material is utilized for booth elastic and plastic deformations perpendicular to the grain. The most commen model for modeling orthotropic materials in plastic condition is based on the Hill yield criterion. This model is developed for metals and do not account for plastic volume changes. Because of the plastic volume change is a key feature of wood a foam model will be used in this thesis which takes this into account. It has the disadvantage, on the other hand, of being based on isotropic behavior of the material [8]. Therefore two material models will be used in this thesis, one which captures the ortotropic elastic behavior in the longitudinal direction and another one which captures the elastic and plastic behavior in radial and tangential direction.

The linear elastic model is created with engineering constants as an orthotropic material (compare matrix C at page 7) but will not take any loads in radial and tangential direction, see *table 7.4*. The loads in these directions will be handled by the elastic-plastic non linear material model. The intial values are taken from Persson's doctoral thesis [16] and can be seen in *table 7.3*.

The non linear model has been created as an isotropic elastic material (see *table 7.5*) with a material addition to handle the plastic behavior, called crushable foam hardening. The crushable foam hardening is based on the assumption that the resulting deformation is not recoverable instantaneously and can be idealized as plastic for short duration events [16]. The hardening curve is described by the uniaxial compression yield stress as a function of the corresponding plastic strain,

see *table 7.6* and *table 7.7*. The values in the table have been found using initial values from Rosengren's Master's thesis [18] and Holmberg's doctoral thesis [8]. The values have been refined in this thesis to better correspond with the laboratory results.

Parameter	Value
E_L, MPa	13500 - 16700
E_R, MPa	700 - 900
E_T, MPa	400 - 650
G_{LR}, MPa	620 - 720
G_{LT}, MPa	500 - 850
G_{RT}, MPa	29 - 39
v_{RL}	0.018 - 0.030
v_{TL}	0.013 - 0.021
v_{RT}	0.24 - 0.33

Table 7.3: Stiffness properties of wood (spruce) at moisture content 12 % [16].

Parameter	Value
E_L, MPa	13500
E_R, MPa	0.05
E_T, MPa	0.05
G_{LR}, MPa	600
G_{LT}, MPa	600
G_{RT}, MPa	0.04
v_{RL}	0.02
v_{TL}	0.02
v_{RT}	0.3

Table 7.4: Stiffness properties of the linear elastic material model.

Parameter	Value
E, MPa	250
ν	0.2

Table 7.5: Elastic properties of the non linear material model.

Compression yield stress ratio	Hydrostatic yield stress ratio
1.5	1.0

Table 7.6: Plastic material properties of crushable foam.

Yield stress σ, MPa	Uniaxial plastic strain ϵ, MPa
4	0.0
8	1.0
8.2	1.8
9.5	2.0
16.5	2.1

Table 7.7: Plastic material properties of crushable foam hardening.

7.4 Element mesh

The mesh is the decisive factor that influences the accuracy of the results obtained by the FE-model. For the unreinforced models three-dimensional solid hexagon elements were used for the beam, the support and the loading plate. A conceptual figure of the mesh can be seen in *figure 7.3*. The general element size is chosen to be 0.02 m but in the geometry close to the support where high gradients might occur, the mesh size is intensified and set to 0.01 m in y-direction. The number of elements for each calculation can be seen in *table 7.8* and *table 7.9*.
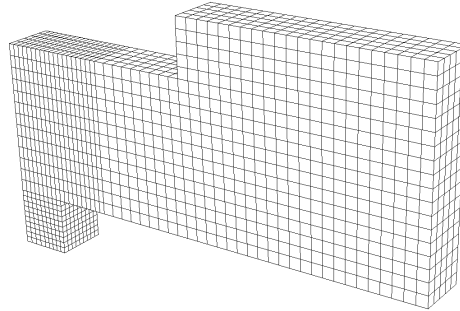
Figure 7.3: A figure showing the element mesh of a beam with dimensions $90x270$.

Unreinforced beams $90x270$					
Support length [m]	Linear model	Non-linear model	Loading plate	Support	Total
0.06	3120	3120	575	540	7355
0.09	3250	3250	550	810	7860
0.12	3315	3315	500	1080	8210

Table 7.8: Number of elements in each part of the 90x270 beams.

Unreinforced beams $115x630$					
Support length [m]	Linear model	Non-linear model	Loading plate	Support	Total
0.06	13632	13632	840	720	28824
0.09	14016	14016	810	1080	29922
0.12	14208	14208	750	1440	30606

Table 7.9: Number of elements in each part of the $115x630$ beams.

7.5 Boundary conditions and loads

The displacement of the loading plate is set to 10 % of beam height, i.e. the steel plate will move 27 mm in negative y-direction for a beam with height 270 mm. All other boundaries are set free on the loading plate including rotational degrees of freedom. In the symmetry plane the displacements in the beams axis (x) and vertical (z) direction are set to zero. The displacements in y-direction and all rotations are set to move freely. The supports bottom side is set to 'Encastre', which means that all translational degrees of freedom are set to zero on this surface.

(a) Load   (b) Symmetry   (c) Support
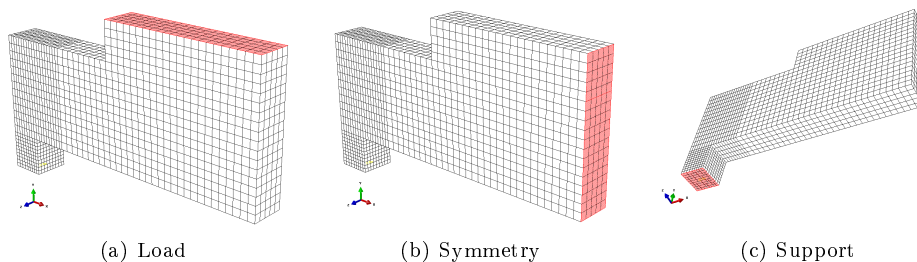
Figure 7.4: Applied boundary conditions.

7.6 Interactions

The contact surface between the loading plate and the beam is modeled by tangential friction (friction in the contact surface plane between the beam and supoort) and is set to 0.19. The reason for putting the tangential friction to 0.19 is that the calculations goes a lot faster using symmetry in the stiffness matrices [20]. In the normal direction of the contact surface plane a 'Hard contact'-relationship is used to transmit the contact pressure between the surfaces. The same interaction is set on the surface between the beam and the support.

To combine the two material models (linear and non-linear for the beams) a constraint called 'Embedded region' was used. This constraint makes, simplified, the

two material models work as one. The linear model works as a host for the embedded non-linear material. ABAQUS searches for geometrical relationships and to avoid topology issues each element mesh for the two material models is meshed identical. The embedding eliminates the translational degrees of freedom of the nodes in the non linear model and they become embedded with the host [20].

To register the reaction force in the support a constraint called coupling was used which means that all nodes on a specific surface is locked to a single node. In this unique node is it possible to read the summarized reactions for all nodes as one reaction force.

7.7 Results and conclusions

This chapter is allocated to the unreinforced model and comparison with the laboratory tests made by Edh and Hasselqvist [5]. Further the models are compared and summarized to analyze the affect of three different support lengths. The unreinforced models are shown below with different beam dimensions and different support lengths.

7.7.1 Beam $90x270$

There were two different dimensions tried out, $90x270$ and $115x630$ mm^2 to see if, and in that case how, the height and/or width affects the stiffness perpendicular to the grain. Stress perpendicular to the grain (y-axis) is calculated by dividing reaction force with support area. The deformation is calculated by measuring the node displacements in the beam at the support.
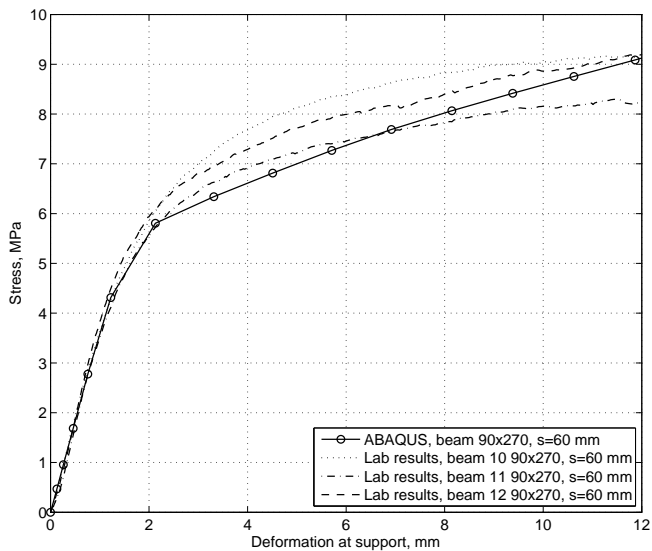
Figure 7.5: Comparison between ABAQUS model and labratory tests, beam $90x270$ support length 60 mm.
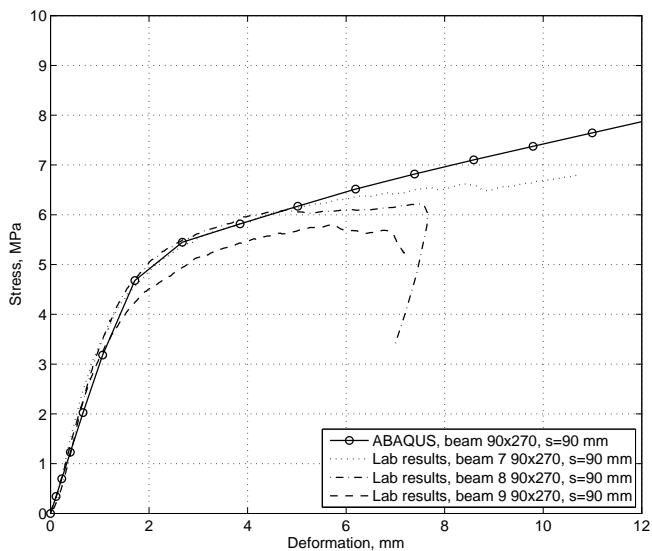
Figure 7.6: Comparison between ABAQUS model and labratory tests, beam $90x270$ support length 90 mm.
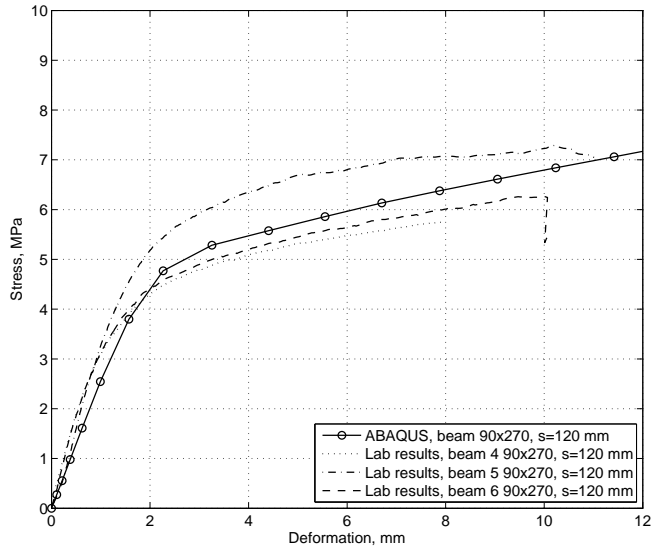
Figure 7.7: Comparison between ABAQUS model and labratory tests, beam $90x270$ support length 120 mm.
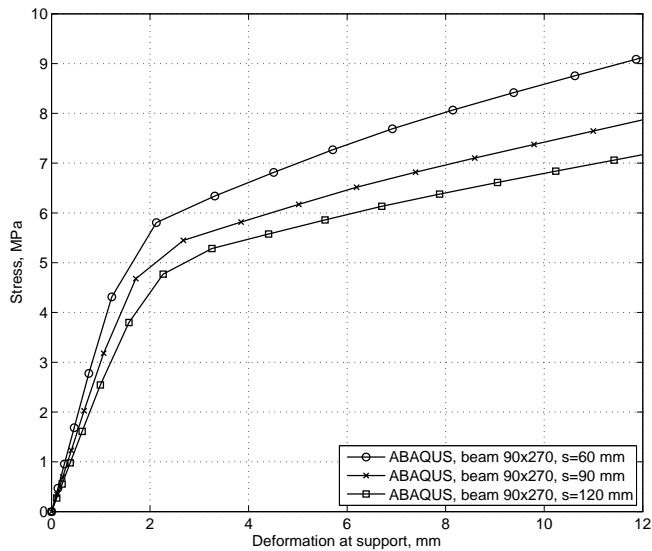
Figure 7.8: Comparison between different support lengths, ABAQUS beam $90x270$.

The FEM-models agree with the lab results. The plastic behavior is captured. It can be seen in *figure 7.8* that there clearly is a connection between stiffness and support length. As the support length decrease the elastic stiffness increase. The beam with support length 60 mm reaches 5.8 MPa before the elastic stiffness decreases and plasticity occurs. It can also be shown that the elastic part of deformation is stiffer when using 60 mm support compared to 120 mm.

7.7.2 Beam 115x630

Just as the three previously models these models with dimension 115x630 mm^2 will be modeled with different support lengths to identify the effect.
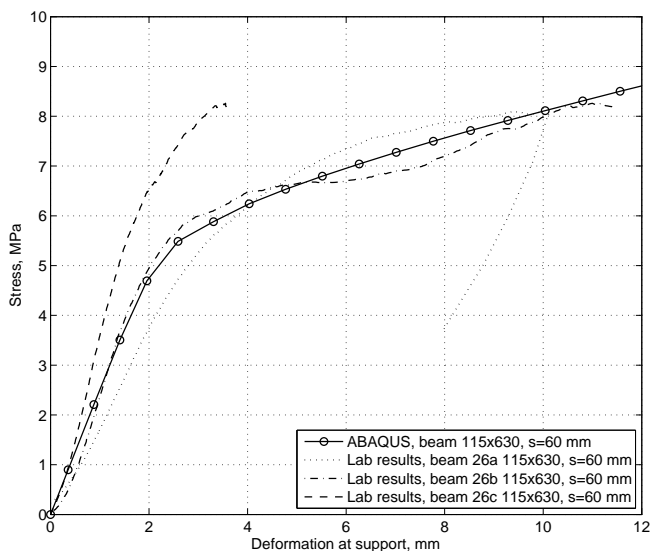
Figure 7.9: Comparison between ABAQUS model and labratory tests, beam 115x630 support length 60 mm.
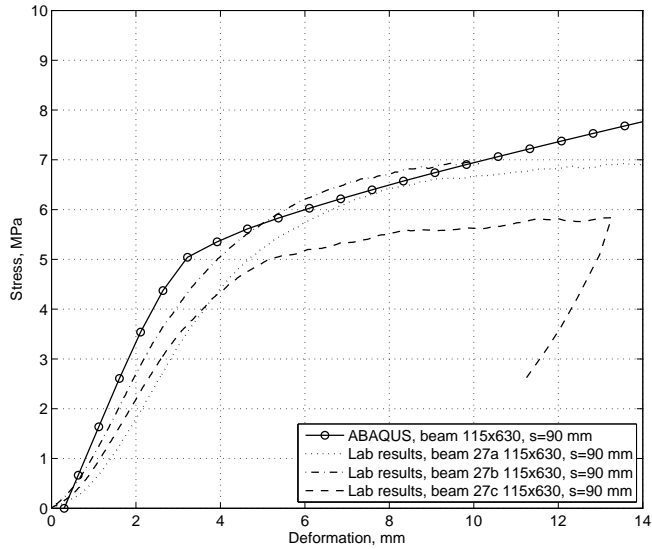
Figure 7.10: Comparison between ABAQUS model and labratory tests, beam $115x630$ support length 90 mm.
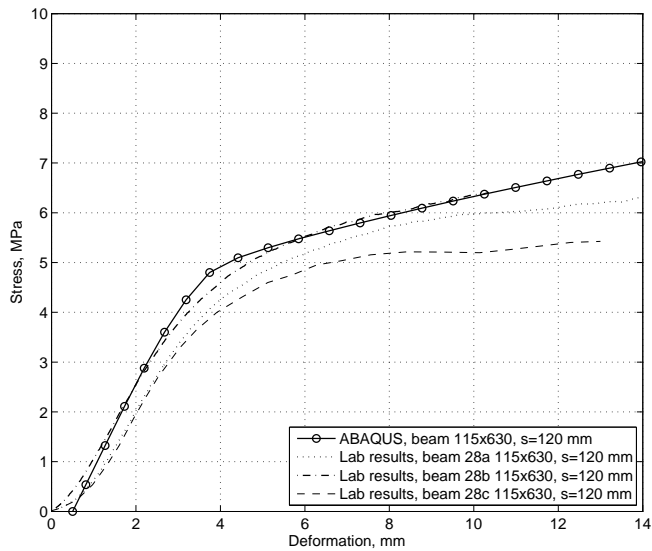
Figure 7.11: Comparison between ABAQUS model and labratory tests, beam $115x630$ support length 120 mm.
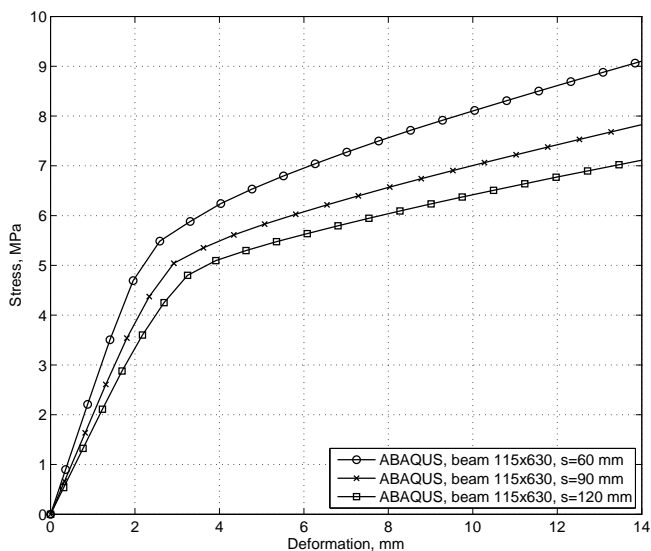
Figure 7.12:   Comparison between different support lengths, ABAQUS beam $115x630$.

The unreinforced $115x630$ FE-model corresponds well with the lab results when the support length is 60 mm. When the FE-model is compared to lab results in support length 90 mm and 120 mm the FE-model behaves a bit stiffer than the test beams. A possible cause is that the densities of these beams are below average.

A comparison between the $90x270$-beams and the $115x630$-beams shows that the heights of the beams have little impact on the results, see *figure 7.13*.

To compare the FE-results with the example made in chapter 3 the FE-results must be translated according to the method described in chapter 3.2 'Definition of the load carrying capacity'. This shows that the capacity perpendicular to the grain according to the FE-models is 72 kN which is larger than Eurocode 5 (47 kN) but lower than BKR 13 (83 kN). The reduction of f_{c90k} from 8 MPa to 2.7 MPa seems a bit too conservative according to the results in this thesis.

7.8   Calculating a new increase factor, $k_{c,90}$

7.8.1   Method

By viewing the results from the FE-models it is obvious that $k_{c,90}$ varies by different support lengths under 400 mm. In *figure 7.12* it seems that a decreasing support length increases the stiffness. With FE-models which captures the behavior it is possible to model beams with other support lengths than 60, 90 and 120 mm. To
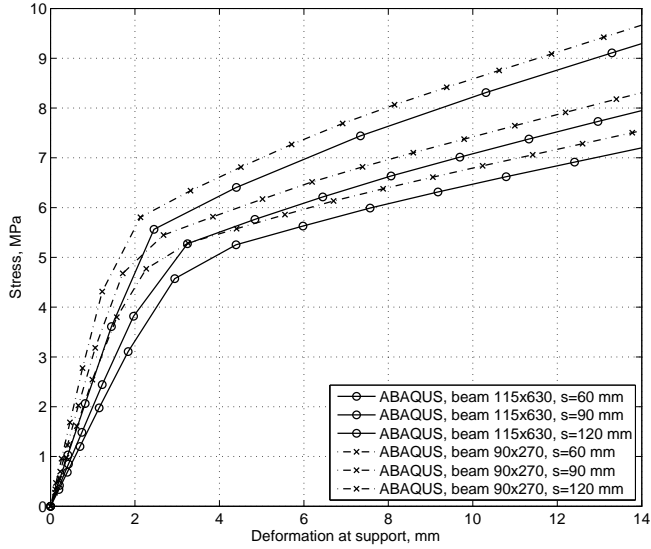
Figure 7.13: Comparison between the $115x630$ beams (solid line) and the $90x270$ beams (dashdotted line) with support lengths 60, 90 and 120 mm.

see how the stress and deformations behaves four new setups will be modeled with geometry according to *figure 7.2* and *table 7.10*. The length of the beams is 4 m. l_A and l_B still depends on *equation 7.3* and the number of elements in every calculation is found in *table 7.11*.

$l_{support}$[mm]	l_A[mm]	l_B[mm]
100	730	1270
200	830	1170
300	930	1070
400	1030	970

Table 7.10: Dimensions depending on different support lengths.

Unreinforced beams $115x630$					
Support length [m]	Linear model	Non-linear model	Loading plate	Support	Total
0.1	21312	21312	1920	1200	45744
0.2	22080	22080	1740	2400	48300
0.3	23232	23232	1620	3600	51684
0.4	24192	24192	1470	4800	56654

Table 7.11: Number of elements in each part of the $115x630$ setups.

The stress-deformation behavior for all tried out support lengths is plotted in a common plot. A designer would be interested by the stress levels and total acceptable deformation depending on the support length. To make a plot of these two variables four vertical lines are drawn in a stress-deformation plot. Where the vertical lines intersect the stress-deformation functions the stress value is read. With the stress values, support length and the deformation a new plot can be created with stress on the y-axis and support length on the x-axis. It is then possible for a designer to see allowed stress levels depending on deformation requirement and length of the support.

For calculation of the increase factor k_{c90} the stress values in the previous plot are found by using the Eurocode 5 equation:

$$\sigma_{c90} < k_c \, f_{c,90} \tag{7.4}$$

$$\Longleftrightarrow$$

$$\frac{\sigma_{c90}}{f_{c,90}} = k_c \tag{7.5}$$

The k_c-values are then plotted with support lengths 100-400 mm. From there it is possible to approximate a linear function by using the highest and lowest k_c-values with corresponding support lengths.

7.8.2   Results
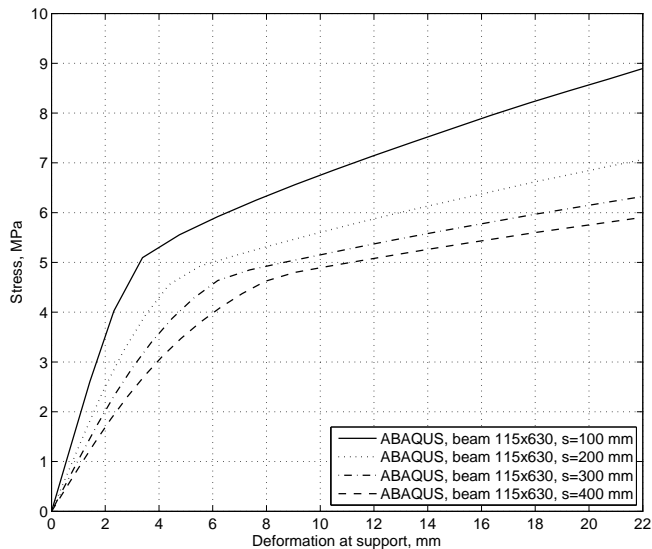
Figure 7.14: Stress-deformation plot for support lengths 100-400 mm.
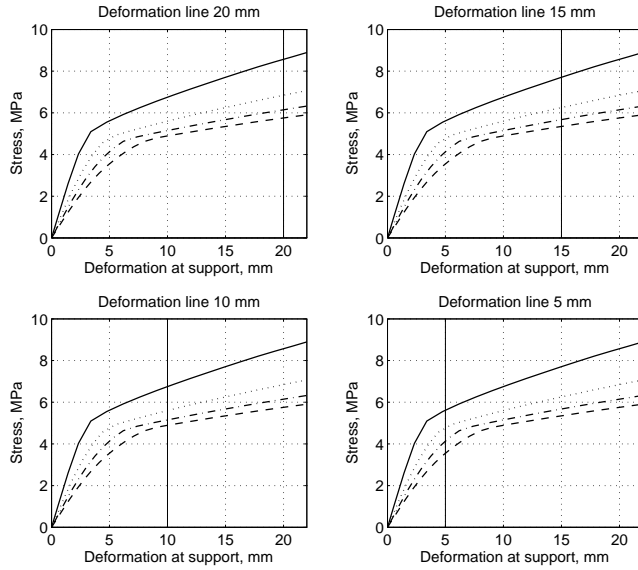
Figure 7.15: Four vertical lines defining deformation requirements 5-20 mm in vertical y-direction.
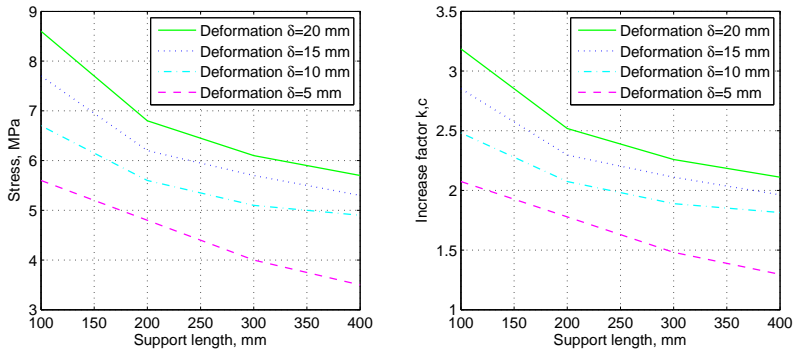
Figure 7.16: To the left: different deformations as a function of stress levels and support length and to the right: different deformations as a function of the increase factor k_{c90} and support length.

What can be seen from *figure 7.16* is that it is hard to decide one general factor k_c without defining a certain allowed deformation magnitude. Because of the level of acceptable deformation is a matter between the designer and a client (as mentioned in chapter 3), a general k_c would not help that case. It is more giving for a designer using *figure 7.16* where the stress levels are plotted with deformation and support lengths.
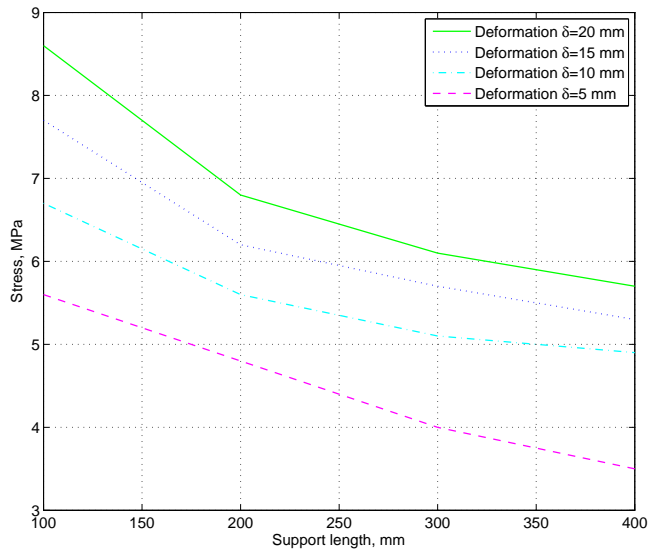
Figure 7.17: Different deformations as a function of stress levels and support length.

So if you are a designer and having a displacement requirement of 10 mm and a column cross section of $115x115$ the maximum stress level accepted is 6.6 MPa.

Chapter 8

The models for reinforced wood

In this chapter the unreinforced FE-models are presented and compared with lab results just like in previous chapter. There are two types of reinforcement, wooden dowels and threaded rods made by steel. Later in the chapter the reinforced FE-models are compared to the unreinforced to illustrate if there are any differences.

8.1   Assumptions and limitations of the FE-model

The same assumptions and limitations as in previous chapter, the unreinforced models, applies in this section. The screws are modeled as cylinders due to modeling the threads for the screws would have taken to long time. This assumption neglects any extra friction between the screw and the glue. The glue is modeled as a homogeneous membrane around each screw.

8.2   Geometry

Just like the beams in previous chapter, due to symmetry, only half of the beams will be modeled and tested with different support lengths. The reinforced beams have the dimensions $115x630mm^2$ and consist of two different types of reinforcement, wood and steel. For support 60 mm there are 2 reinforcing bars, 90 mm 4 bars and finally 120 mm 6 bars. The height h_{reinf} is 400 mm for all models. The geometry reminds of the unreinforced, see *figure 8.1*, *figure 8.2*, *table 8.1* and *table 8.2*.
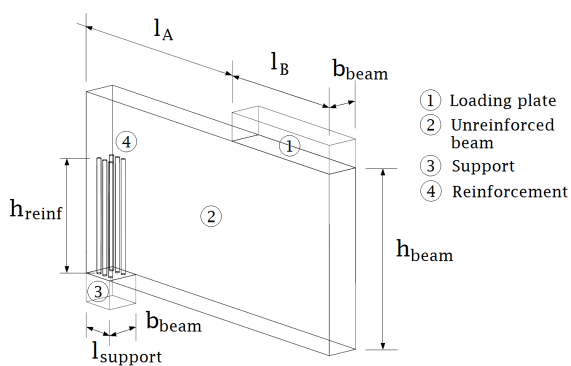
Figure 8.1: Geometry of the unreinforced beams.
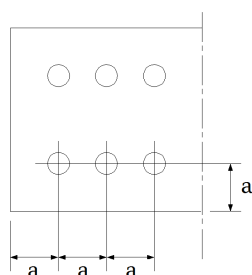
Figure 8.2: Geometry of the unreinforced beams.

l$_{support}$ [mm]	l$_A$ [mm]	l$_B$ [mm]	a [mm]	No. of dowels [ ]
60	690	560	30	2
90	720	530	30	4
120	750	500	30	6

Table 8.1: Dimensions depending on different support lengths.

l$_{support}$ [mm]	l$_A$ [mm]	l$_B$ [mm]	a [mm]	No. of threaded rods [ ]
60	690	560	30	2
90	720	530	30	4
120	750	500	30	6

Table 8.2: Dimensions depending on different support lengths.

8.3   Materials

The materials of loading plate, beam and support are the same as in the unreinforced models. The reinforcement dowlings are made of birch and the threaded dowels, type M12 4.6, are made of steel. Worth noticing is that birch have almost same Youngs modulus in longitudinal direction as spruce [9]. The bonding between the beam and the reinforcement is modeled with glue. The material properties for birch, steel and glue can be seen in *table 8.3*, *table 8.4* and *table 8.5* respectively.

Parameter	Value
E_L, MPa	14000
E_R, MPa	1100
E_T, MPa	630
G_{LR}, MPa	740
G_{LT}, MPa	950
G_{RT}, MPa	140
v_{RL}	0.02
v_{TL}	0.02
v_{RT}	0.3

Table 8.3: Material properties of birch at 12 % moisture content [9].

Parameter	Value
E, GPa	210
ν	0.3
f_{yk}, MPa	240

Table 8.4: Material properties of threaded rod M12 4.6.

Parameter	Value
E, MPa	1000
ν	0.3

Table 8.5: Material properties of glue (dry) [17].

8.4   Element mesh

The meshing procedure reminds of the unreinforced and the differences relates to the reinforcement. In *figure 8.3* and *figure 8.4* a conceptual view over the mesh is shown. To model the glue between the bars and the cylindrical walls in the beam cohesive element were used. Cohesive elements are used to model, for example, adhesive joints between two components, fracture at bonded interfaces or gaskets [20]. Meshing the cohesive elements in radial direction defines the material

orientation and also the thickness layer. The thickness layer is set to 1 mm for both dowels and threaded rods. When modeling the reinforcements made of wood there had to be two different local coordinate systems, one coordinate system for the cohesive elements and another coordinate system do define woods orthotropic behavior. The number of elements for each calculation can be seen in *table 8.6* and *table 8.7*. A quick comparison between the dowel and rod models shows that there are low differences in numbers of element.
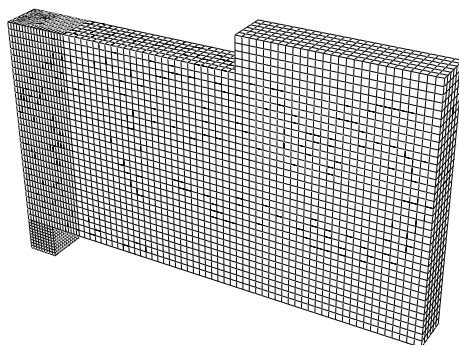
Figure 8.3: Mesh over the setup.
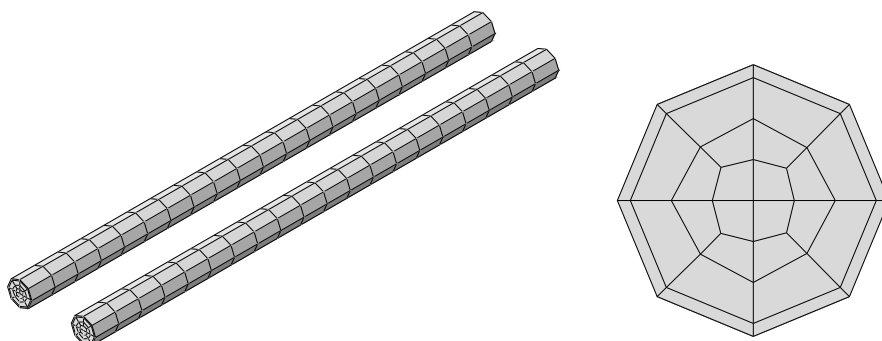
Figure 8.4: An overview over the reinforcement mesh.

Reinforced beams $115x630$							
Support length [m]	Linear Model	Non-linear Model	Loading plate	Support	Reinforcement		Total
					Hex	Cohessive	
0.06	14528	14528	840	1590	800	320	32606
0.09	17888	17888	810	2850	1600	640	41676
0.12	21728	21728	750	4230	2400	960	51796

Table 8.6: Beam model reinforcement dowels ($115x630$)

Reinforced beams 115x630							
Support length [m]	Linear Model	Non-linear Model	Loading plate	Support	Reinforcement		Total
					Hex	Cohessive	
0.06	14238	14238	840	1590	800	320	32026
0.09	17530	17530	810	2850	1600	640	40960
0.12	21294	21294	750	4230	2400	960	50928

Table 8.7: Beam model reinforcement threaded rods (115x630)

8.5 Boundary conditions and loads

The boundary conditions are exactly the same as in the unreinforced models, see chapter 7.5. The displacement of the loading plate is set to 10 % of every beams height which is equivalent to 63 mm in the reinforced models.

8.6 Interactions

The friction, embedding and coupling are exactly the same as in the unreinforced models. The interaction between the glue and the beam is modeled with a 'Tie constraint'. A tie constraint means that two regions/surfaces is fused together i.e. the translational and rotational motion as well as all other active degrees of freedom for a pair of surfaces is equal [20]. The glue is modeled with a finer element mesh and therefore set to slave. The choice of master and slave is based on the cohesive zone being composed with a softer material and having a finer discretization. A second consideration also suggests that mismatched meshes will be used and because of that, the pressure distribution on the cohesive elements may be predicted inaccurately.

8.7 Results and conclusions

Just like with the unreinforced FE-models, the models are compared to lab results to verify that they captures the real behavior.

8.7.1 Beams reinforced with dowels

The wood reinforced beams were some of irregular at the contact zone between the beam and the support. It is visualized in *figure 8.6* as the stiffness curve behaves non linear at very small deformations. The linear behavior occurs after a deformation of 0.5 mm. The model in ABAQUS however is pure planar at the contact zone and to compare the model with the laboratory testing this curve was adjusted 0.5 mm to the right to fit the linear elastic of the laboratory testing

The FE-models with wood reinforcements seem to catch the actual behavior from the tested reinforced beams. The stiffness in the elastic area correlates very well. There are however some differences when comparing the support length 90 and 120 mm. As can be seen in *figure 8.7* and *figure 8.8* the FE-models do not reach above 12 MPa like the tested specimens do. A possible cause can be that the reinforced wood columns have a higher yield point before entering plastic behavior. In this model the yield point for load parallel the grain is 60 MPa and in reality it could be higher. The beams with support 90 and 120 mm with $\sigma_{yield} = 80$ MPa, is plotted in *figure 8.9* and *figure 8.10*.

Another remark of this comparisons is that when the specimens capacity is drained and the curve slops the FE-models continue to carry load. This effect is due to cracks appears in the specimens which reduces the horizontal stiffness and therefore the dowels buckles. Crack propagation is not taken into account in this thesis.
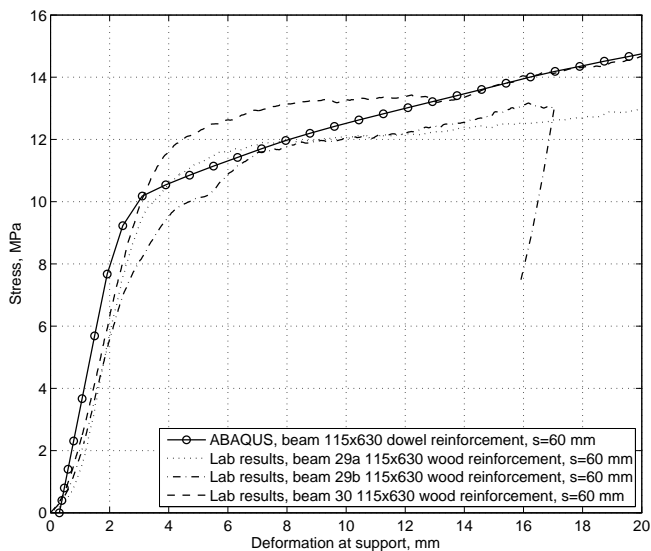
Figure 8.5: Comparison between ABAQUS model and laboratory tests, beam $115x630$ with dowels support length 60 mm.
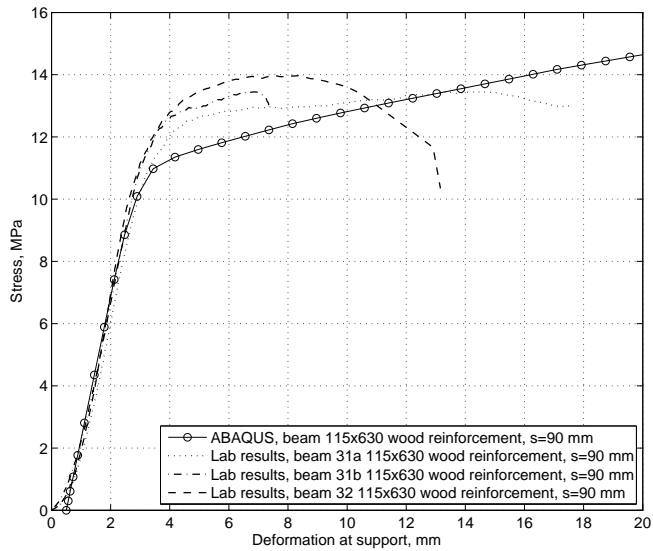
Figure 8.6: Comparison between ABAQUS model and laboratory tests, beam $115x630$ with dowels support length 90 mm.
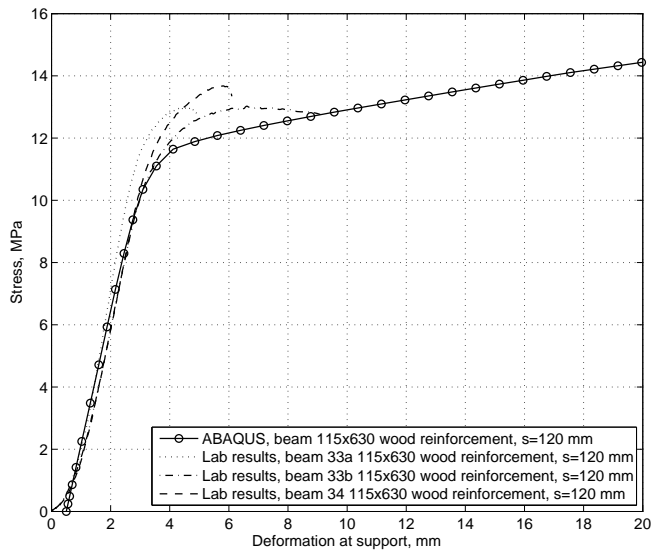
Figure 8.7: Comparison between ABAQUS model and laboratory tests, beam $115x630$ with dowels support length 120 mm.
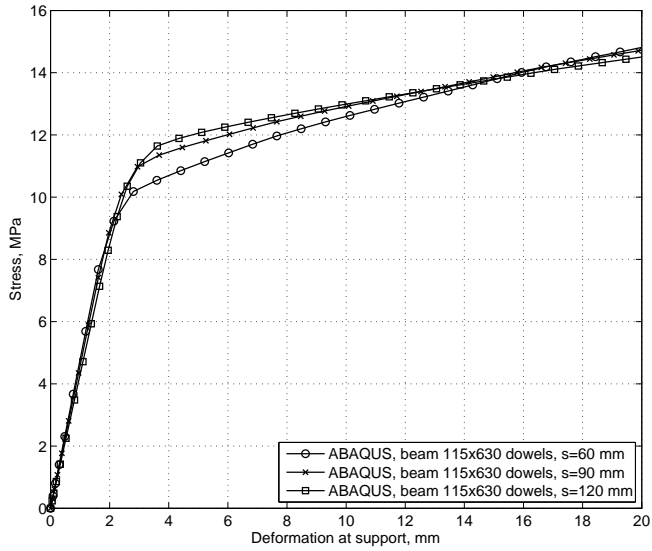
Figure 8.8: Comparison between reinforced beams with dowels in different support lengths.
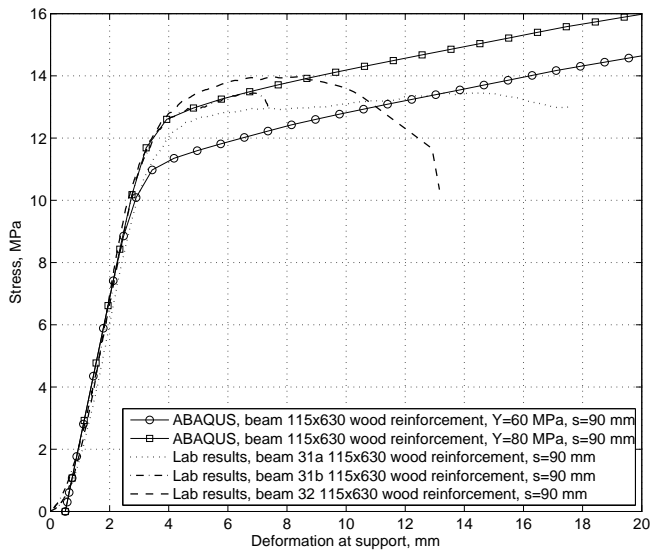
Figure 8.9: Illustrating the new yield point 80 MPa in longitudinal direction for the reinforcing dowels, support length 90 mm.
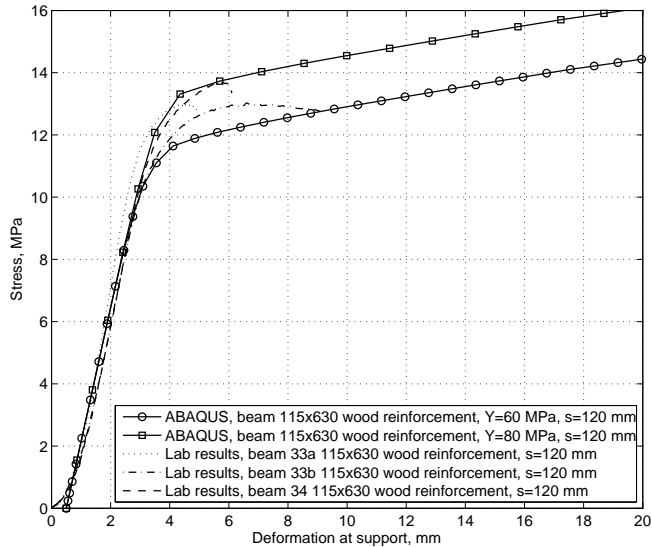
Figure 8.10: Illustrating the new yield point 80 MPa in longitudinal direction for the reinforcing dowels, support length 120 mm.

8.7.2 Beams reinforced with threaded rods

The steel reinforced beams are also tried out with different support lengths to see if the length affects the stress capacity perpendicular to the grain. In chapter 5 (Laboratory testing), the pictures shows that there is at least 2 mm gap between the end of a screw and the underside of the beams. Overall, the gap varied irregular from 2 mm up to 8 mm. These values were not saved which have led to challenges in modeling. It is too time-consuming to test all different combinations with trial and error so a simplified approach have been applied. To capture the influence of the gap each reinforced steel beam has been modeled in two sets; with no gap and a gap of 2 mm.

In *figure 8.11* above there is only one FEM-model plotted due to it is clear that the model do not capture the lab results. In the figure it is observed that the screws yield point is too low (240 MPa) and that the slope of the curve decreases. To better capture the behavior a new yield point is set to 400 MPa as in the article by Bejtka and Blass [22]. Evaluation of this yield point is shown in *figure 8.12*.
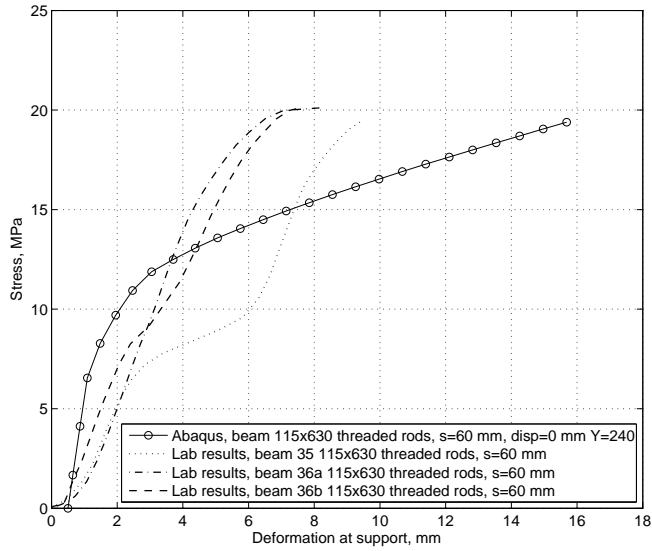
Figure 8.11: Comparison between ABAQUS model and labratory tests, beam 115x630 with threaded rods support length 60 mm.
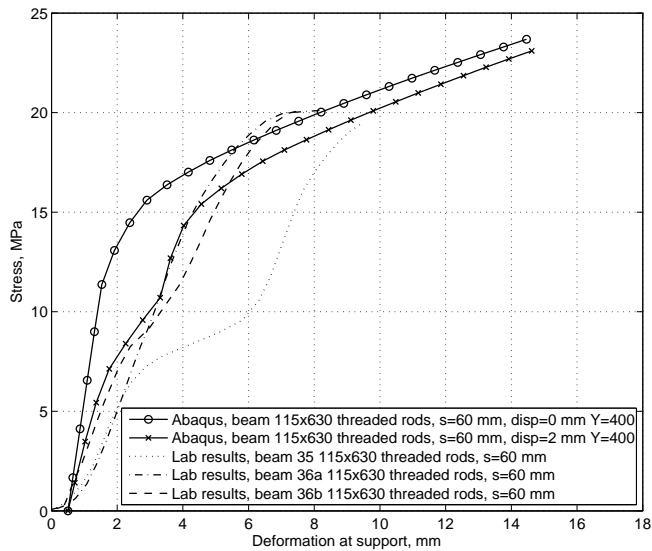
Figure 8.12: Comparison between ABAQUS model and labratory tests, beam $115x630$ with threaded rods support length 60 mm with new yield point.

It is clear that yield point 400 MPa captures the lab results a lot better than the first assumption regarding the yield point. For further models, yield point 400 MPa is used.
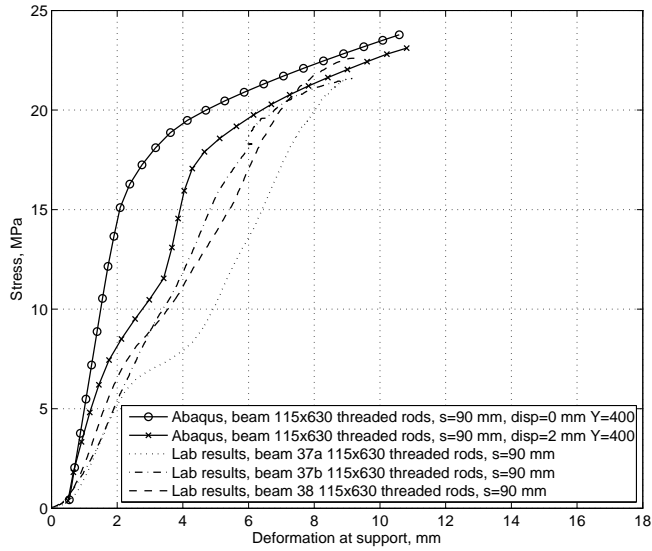
Figure 8.13: Comparison between ABAQUS model and labratory tests, beam $115x630$ with threaded rods support length 90 mm.
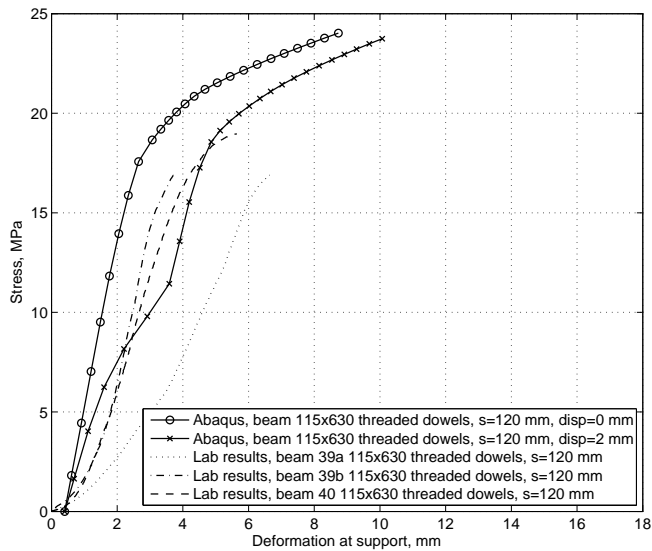
Figure 8.14: Comparison between ABAQUS model and labratory tests, beam $115x630$ with threaded rods support length 120 mm.
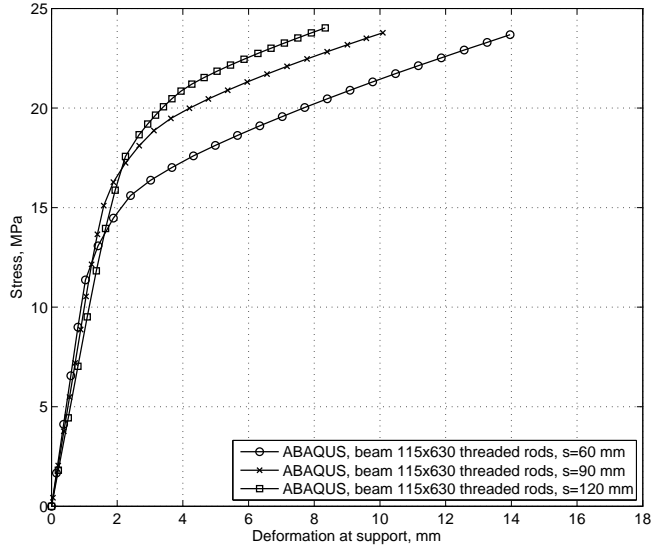
Figure 8.15: Comparison between reinforced beams with threaded rods in different support lengths.

It is clear that the model with 2 mm displacement captures the stress-deformation results from the lab tests better than the model without displacement. Especially where the support length is 60 mm, see *figure 8.13*. In the models with support length 90 and 120 mm there are deviations but this probably depends on the gap between the screws and the support varies in between 2-8 mm. As stated above, this is too time-consuming to model. Another remark of this comparisons is that when the specimens capacity is drained and the curve slops the FE-models continue to carry load. This effect is due to cracks appears in the specimens which reduces the horizontal stiffness and therefore the screw buckles. Crack propagation are not been taken into account in this thesis. The stress perpendicular to the grain and the deformation is illustrataded in *figure 8.16* and *figure 8.17* respectively.
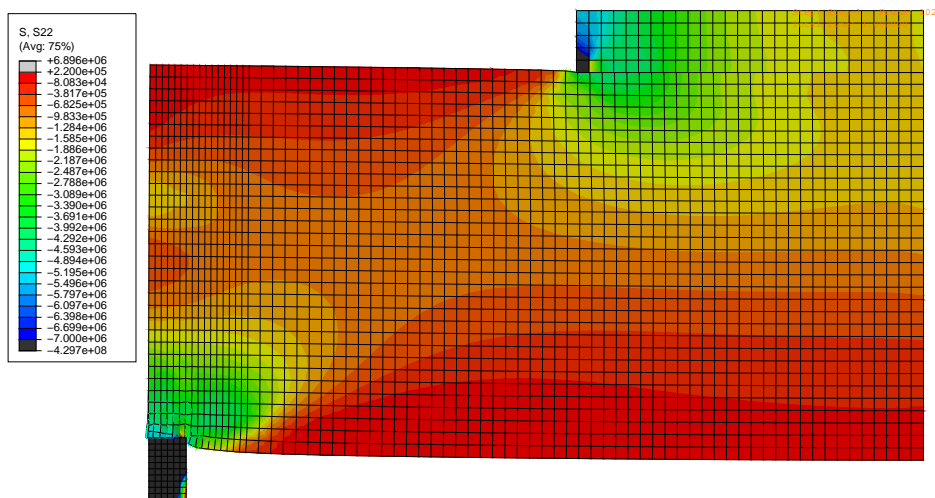
Figure 8.16: Stress perpendicular to the grain in the reinforced beam.
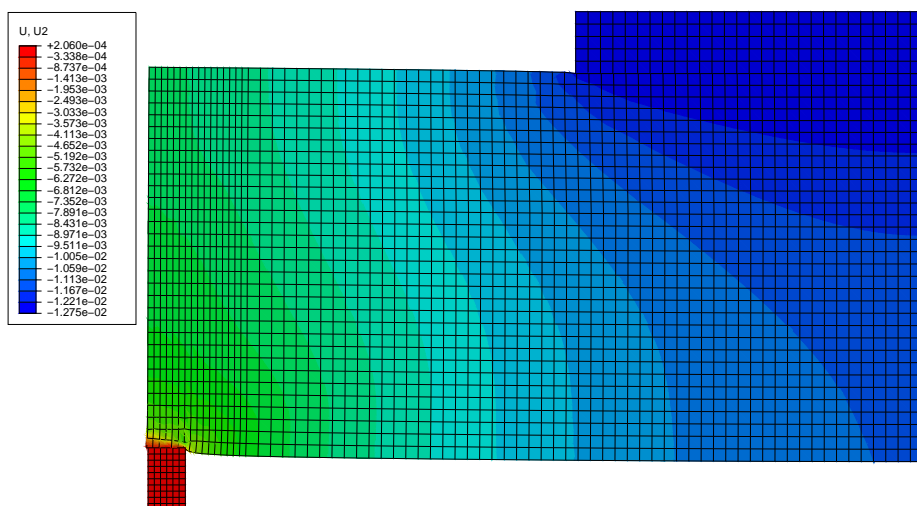
Figure 8.17: The displacements in vertical direction.

It is of interest to see how how the screws behaves in the FE-models. In *figure 8.18* a von Mises-plot over the screws in the FE-model just when the screws in the specimen buckles. The FE-model, as stated above, does not take cracks into account which makes the horizontal stiffness foundation stiffer compared to in the specimen.
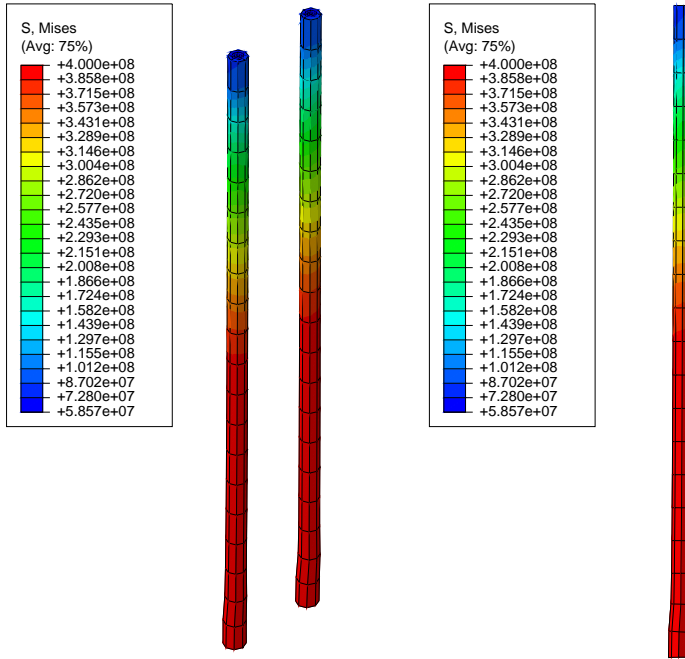
Figure 8.18: von Mises stresses (Pa) in the threaded rods. To the left a 3D-view and to the right a 2-D view to illustrate the deformations.

Because of the FE-models do not capture the cracking behavior it is complicated to specify a specific stress capacity for both the dowels and the threaded rods. The FE-models of beams reinforced with dowels captuers the elastic behavior very well however so the capacity for the dowels will be handled only in the elastic part. The threaded rods behavior in the elastic area were hard to capture even with a 2 mm displacement due to the irregular gaps between the rods and the support. However the models shows there is clearly a benefit in deformations if the beams would be produced with no gap at all. In all stress-deformation graphs for the rods there is a obvious difference in deformations between the models having no gap and models with a gap of 2 mm. If the rods would be placed at the exact same level as the bottomside of the beam it would increase the stiffness alot according to the FE-models. Yet it would be of impartance to produce the beams with precision. If the rods stick out just some mm's from the bottomside of the beam the rods will carry all load by themselves.

The reinforced beams with dowels behaves elastic until stress rate is 10.2, 11.1 and 11.5 MPa (see *figure 8.8*) is reached for support lengths 60, 90 and 120 mm respectivly. Compared with the model developed by Blass and Betjka (see chapter 4) the values are higher than Eurocode 5 (7.7, 8.4 and 8.8 MPa) but lower than the BKR 13 (15.6, 15.5 and 15.4 MPa). A possible cause is that the model is developed for self-tapping screws and the foundation stiffness is different. Compared to the

Eurocode 5-values there is an average increase of capacity of 32 %. To get a better overview the results are presented in *table 8.8*.

The model developed in Karlsruhe do not take any gap into account so it is possible to compare the these reults with the FE-results. This comparison will, just like with the dowels, only handle the elastic part of the deformations. The reinforced beams with threaded rods behaves elastic until stress rate 11.0, 15.1 and 17.8 MPa (see *figure 8.15*) is reached for support lengths 60, 90 and 120 mm respectivly. Just like with the dowels the FE-values are compared to the calculations in chapter 4.5. The calculated values are 12.1, 14.4 and 15.5 MPa (Eurocode 5) and 20.1, 21.4, 22.1 MPa (BKR 13). Compared to the Eurocode 5-values there is an average increase capacity of 4 %. To get a better overview the results are presented in *table 8.8*.

| Stress capacity [MPa] | Reinforcement | | | | | |
	Dowels			Threaded rods		
Support length [mm]	60	90	120	60	90	120
Eurocode 5	7.7	8.4	8.8	12.1	14.4	15.5
BKR 13	15.6	15.5	15.4	20.1	21.4	22.1
FE-models	10.2	11.1	11.5	11.0	15.1	17.8
FE-models / Eurocode 5	1.32	1.32	1.31	0.92	1.05	1.15
FE-models / BKR 13	0.65	0.72	0.75	0.55	0.71	0.81

Table 8.8: Comparison between the FE-models and calculations from chapter 4

The model developed in Karlsruhe have been designed for handling self-tapping screws up to 12 mm of diameter which can explain that there are differences in the results but overall BKR 13 have values which are a bit too high compared with the FE-models.

8.7.3 Comparison between the unreinforced and reinforced models

Comparisons in stress-deformation between the reinforced and unreinforced models are illustrated in *figure 8.19*. It is clear that the reinforcement makes the beam a lot stiffer in stress perpendicular to the grain. At a deformation of 2 mm the unreinforced beams have an average stress capacity of 4 MPa. This value can be compared with the reinforced beams where the stress magnitude is 8 MPa and 16 MPa. Reinforcing with dowels doubles the stress capacity perpendicular to the grain and reinforcing with threaded rods makes the capacity four times larger than unreinforced.
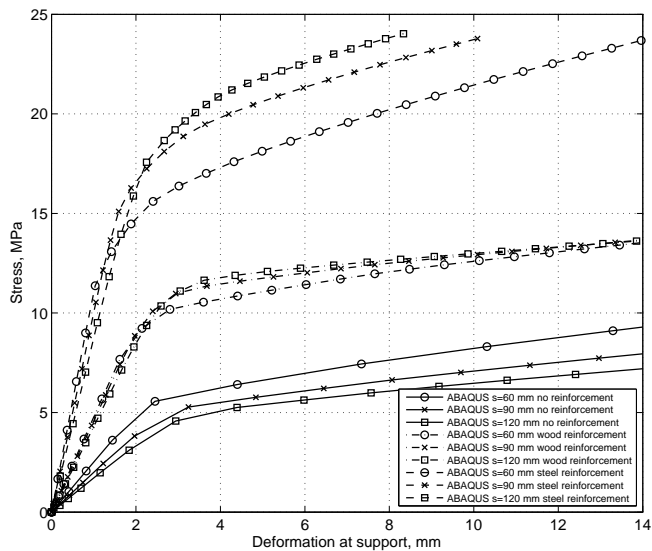
Figure 8.19: Comparison between the reinforced beams and unreinforced $(115x630)$.

Chapter 9

Final remarks

In this thesis it has been shown that decreasing support length under 400 mm increases the stiffness perpendicular to the grain. The value in Eurocode 5 is conservative as recommending a characteristic compression capacity of 2.7 MPa. The FE-models show that the neighboring unloaded parts of the beam helps transferring the stresses. The capacity varies with different support length and allowable deformations. If a designer allows a deformation of 20 mm, independent of beam height, and using a support length of 100 mm the characteristic capacity would be 8.7 MPa which is about three times larger than the values proposed in Eurocode 5. However, if a designer allow a deformation of 5 mm and using a support length of 400 mm the capacity is only 2.1 MPa which is lower than the Eurocode 5 value. Different functions of acceptable deformation are plotted as functions of support length and stress level which would come handy for a designer to use.

The analysis of reinforcing with wooden dowels or threaded steel screws points that the reinforcement have a positive effect on the increase of compressive capacity perpendicular to the grain. Due to steels stiffness the threaded rods reach an "elastic capacity" of an average of 16 MPa which can be compared to the wooden dowels which reach an average of 8 MPa. Because of crack propagation has not been taken into account in this thesis the non linear behavior of the reinforcing models is hard to predict. It has also been shown that the model developed in Karlsruhe for reinforced cross sections needs refining for capturing wooden dowels and threaded rods behavior according to the FE-results.

Chapter 10

Future research

During the work it has come up areas which is too time consuming and/or too complicated to model within the limits of the present study and needs further investigations:

- In this thesis neither the lamellas nor the annual rings have been modeled. It is unknown if modelling the lamellas effect the capacity. The annual rings have an effect on the capacity perpendicular which could be seen in chapter 2. But it is unknown how much so this should be analyzed further.

- When modeling the reinforced beams crack propagation is not considered. This has an effect when a dowel or rod is about to buckle. If not cracks are considered the beam continue to carry load but in real life the beam cracks and the dowel or rod buckles.

- In the parallel thesis [5] there were also another type of reinforcement tried out, nailed plates. The nailed plates increased maximal capacity significant due to the load was transferred by the nails and plate. The steel plate also prevented the beam to deform in tangential direction. This is an common connection between beams and columns so a model should be of interest for timber structural designers.

Chapter 11

Bibliography

Books and reports

[1] BFS 2010:2 BKR 13 (2010). *Boverkets konstruktionsregler*. Boverket. Sweden.

[2] Carling, O. (2001). *Limträhandboken*. Svenska limträ AB. Sweden.

[3] Edlund, B. (1995). *Timber engineering- step 1*. Salland De Lange. Netherlands.

[4] Eurocode 5

[5] Edh, D., Hasselqvist, F., (2011) *Timber compression strength perpendicular to the grain - Testing of glulam beams with and without reinforcement*. Lund Institute of Technology. Sweden.

[6] Formolo, S., Granström, R. (2007). *Compression perpendicular to the grain and reinforcement of a pre-stressed timber deck*. Chalmers University of Technology. Sweden.

[7] Green, D,W., Winandy, J.E., Kretschmann, D.E. (1999). *Wood handbook: Wood as an engineering material*. Forest Products Laboratory. Gen. Tech. U.S.A.

[8] Holmberg, S. (1996). *Deformation and fracture of wood in initial defibration processes*. Lund University of Technology. Sweden.

[9] Keylwerth, R. (1951). *Die anisotrope Elastizität des Holzes und der Lagen-hölzer*. VDI Research report 430. Germany.

[10] Johannesson, B. (1984). *Brottkriterier för trä*. Studentlitteratur. Chalmers Institute of Technology. Sweden.

[11] Madsen, B., Leijten AJM, Gehri E, Mischler A, Jorissen AJM (2000). *Behavior of Timber Connections*. First edition, Timber Engineering Ltd. U.S.A.

[12] Osuuskunta, M. (2009). *Analysis of compression perpendicular to grain tests of large glulam beams*. VTT Technical Research Centre of Finland. Finland

[13] Ottoson, N., Petersson, H. (1992). *Introduction to the Finite Element Method.* Pearson Education Limited. England

[14] Ottoson, N., Ristinmaa, M. (2005). *The Mechanics of Constitutive Modeling.* Elsevier Science. U.K.

[15] Ormarsson, S.(1999). *Numerical Analysis of Moisture-Related Distortions in Sawn Timber.* Chalmers University of Technology. Sweden.

[16] Persson, K. (2000). *Micro mechanical modeling of wood and fibre properties.* Lund Institute of Technology. Sweden.

[17] Raknes, E. (1986). *Liming av tre.* Unversitetsforlaget AS, Oslo. Norway.

[18] Rosengren, M. (2010). *Analys av träets tryckhållfasthet vinkelrätt fiberriktningen.* Lund Institute of Technology. Sweden.

[19] SIMULIA, (2011). *ABAQUS/CAE User's Manual version 6.10*

[20] SIMULIA, (2011). *ABAQUS Analysis User's Manual version 6.10*

Articles

[21] Augustin, M., Ruli, A.,Brandner, R., Schickhofer, G. (2006). *Behavior of Glulam in Compression Perpendicular to grain in Different Strength Grades and Load Configurations.* Graz University of Technology. Austria.

[22] Bejtka, I., Blass, H. J. (2006). *Self-tapping screws as reinforcements in beam supports.* Universität Karlsruhe. Germany

[23] Blass, H.J., Görlacher R. (2004). *Compression perpendicular to the grain.* In: Proceedings of world conference timber engineering, vol. 2. Finland.

[24] Colling, F., (2000). *Erhöhung der Querdruckfestigkeit von Holz mittels selbstschneiden Holzschrauben.* FH Augsburg. Germany.

[25] Leijten, A. J. M., Larsen, H.J., Van der Put, T.A.C.M. (2009). *Structural design for compression perpendicular to the grain of timber beams.* Eindhoven University of Technology. Netherlands, Delft University of Technology. Netherlands.

[26] Petersen, T.J. (1999). *Trykpåvirket traes svind og krybning/compressed wood -shrinkage and creep.* Technical University Denmark. Denmark.

[27] Riberholt, H. (2000). *Compression perpendicular to the grain of wood.* COWI-report. Denmark.

[28] Thelandersson, S., Mårtensson, A., (1997). *Design principles for timber in compression perpendicular to the grain.* Lund Institute of Technology. Sweden.

[29] Van der Put, T.A.C.M. (2008). *Derivation of the bearing strength perpendicular to the grain of locally loaded timber blocks.* Faculty of Civil Engineering and Geosciences. Netherlands.

Chapter 12

Appendixes

12.1 Calculations with wooden dowels

KARLSRUHE METHOD WITH WOODEN DOWELS					
	Eurocode 5				
Support length	L=60	L=90	L=120	L=150	L=180
N,ki,k [N]	98 741	98 741	98 741	98 741	98 741
c,h [N/mm2]	176,2	176,2	176,2	176,2	176,2
rho,w [kg/m3]	450	450	450	450	450
alpha	1,57	1,57	1,57	1,57	1,57
E,wood(L) [MPa]	13 500	13 500	13 500	13 500	13 500
I,screw [mm]	4100	4100	4100	4100	4100
k,c90	1	1	1	1	1
f,yk [MPa]	60	60	60	60	60
f,c90,k [MPa]	2,7	2,7	2,7	2,7	2,7
l,screw [mm]	400	400	400	400	400
A,screw [mm2]	227	227	227	227	227
b,beam [mm]	115	115	115	115	115
h,beam [mm]	630	630	630	630	630
l,support [mm]	60	90	120	150	180
l,ef,1 [mm]	90	120	150	180	210
l,ef,2 [mm]	873	903	933	963	993
n	2	4	6	8	10
d,screw [mm]	19	19	19	19	19
d,screw,n [mm]	17	17	17	17	17
lambda,k	0,371	0,371	0,371	0,371	0,371
N,pl,k [N]	13 619	13 619	13 619	13 619	13 619
k	0,611	0,611	0,611	0,611	0,611
kappa,c	0,912	0,912	0,912	0,912	0,912
R,c,k [N]	12 425	12 425	12 425	12 425	12 425
R,ax,k [N]	123 234	229 963	331 238	429 126	524 571
f,ax,k	8,69	8,69	8,69	8,69	8,69
k,d	1	1	1	1	1
n,ef	1,87	3,48	5,02	6,50	7,94
R,k [N]	12 425	12 425	12 425	12 425	12 425
l,ef x b x f,c,90,k	27 945	37 260	46 575	55 890	65 205
n x R,k + l,ef x b x f,c,90,k	52 795	86 961	121 126	155 291	189 457
b x l,ef,2 x f,c,90,k	270 985	280 300	289 615	298 930	308 245
R,90,k [N]	52 795	86 961	121 126	155 291	189 457
f,90,k [MPa]	7,7	8,4	8,8	9,0	9,2

KARLSRUHE METHOD WITH DOWELS					
	BFS 2010:2 BKR 13				
Support length	L=60	L=90	L=120	L=150	L=180
N,ki,k [N]	98 741	98 741	98 741	98 741	98 741
c,h [N/mm2]	176,2	176,2	176,2	176,2	176,2
rho,w [kg/m3]	450	450	450	450	450
alpha	1,57	1,57	1,57	1,57	1,57
E,wood(L) [MPa]	13 500	13 500	13 500	13 500	13 500
I,screw [mm]	4100	4100	4100	4100	4100
k,c90	1	1	1	1	1
f,yk [MPa]	60	60	60	60	60
f,c90,k [MPa]	8	8	8	8	8
l,screw [mm]	400	400	400	400	400
A,screw [mm2]	227	227	227	227	227
b,beam [mm]	115	115	115	115	115
h,beam [mm]	630	630	630	630	630
l,support [mm]	60	90	120	150	180
l,ef,1 [mm]	90	120	150	180	210
l,ef,2 [mm]	873	903	933	963	993
n	2	4	6	8	10
d,screw [mm]	19	19	19	19	19
d,screw,n [mm]	17	17	17	17	17
lambda,k	0,371	0,371	0,371	0,371	0,371
N,pl,k [N]	13 619	13 619	13 619	13 619	13 619
k	0,611	0,611	0,611	0,611	0,611
kappa,c	0,912	0,912	0,912	0,912	0,912
R,c,k [N]	12 425	12 425	12 425	12 425	12 425
R,ax,k [N]	164 307	328 614	492 921	657 228	821 535
f,ax,k	-	-	-	-	-
k,d	-	-	-	-	-
n,ef	-	-	-	-	-
R,k [N]	12 425	12 425	12 425	12 425	12 425
l,ef x b x f,c,90,k	82 800	110 400	138 000	165 600	193 200
n x R,k + l,ef x b x f,c,90,k	107 650	160 101	212 551	265 001	317 452
b x l,ef,2 x f,c,90,k	802 919	830 519	858 119	885 719	913 319
R,90,k [N]	107 650	160 101	212 551	265 001	317 452
f,90,k [MPa]	15,6	15,5	15,4	15,4	15,3

12.2 Calculations with threaded steel rods

KARLSRUHE METHOD WITH THREADED STEEL RODS					
	Eurocode 5				
Support length	L=60	L=90	L=120	L=150	L=180
N,ki,k [N]	127 483	127 483	127 483	127 483	127 483
c,h [N/mm2]	140,1	140,1	140,1	140,1	140,1
rho,w [kg/m3]	450	450	450	450	450
alpha	1,57	1,57	1,57	1,57	1,57
E,steel [MPa]	210 000	210 000	210 000	210 000	210 000
I,screw [mm4]	552	552	552	552	552
k,c90	1	1	1	1	1
f,yk [MPa]	400	400	400	400	400
f,c90,k [MPa]	2,7	2,7	2,7	2,7	2,7
l,screw [mm]	400	400	400	400	400
A,screw [mm2]	83	83	83	83	83
b,beam [mm]	115	115	115	115	115
h,beam [mm]	630	630	630	630	630
l,support [mm]	60	90	120	150	180
l,ef,1 [mm]	90	120	150	180	210
l,ef,2 [mm]	873	903	933	963	993
n	2	4	6	8	10
d,screw [mm]	12	12	12	12	12
d,screw,n [mm]	10,3	10,3	10,3	10,3	10,3
lambda,k	0,511	0,511	0,511	0,511	0,511
N,pl,k [N]	33 329	33 329	33 329	33 329	33 329
k	0,707	0,707	0,707	0,707	0,707
kappa,c	0,837	0,837	0,837	0,837	0,837
R,c,k [N]	27 885	27 885	27 885	27 885	27 885
R,ax,k [N]	97 937	182 756	263 241	341 035	416 887
f,ax,k	10,93	10,93	10,93	10,93	10,93
k,d	1	1	1	1	1
n,ef	1,87	3,48	5,02	6,50	7,94
R,k [N]	27 885	27 885	27 885	27 885	27 885
l,ef x b x f,c,90,k	27 945	37 260	46 575	55 890	65 205
n x R,k + l,ef x b x f,c,90,k	83 714	148 799	213 883	278 967	344 052
b x l,ef,2 x f,c,90,k	270 985	280 300	289 615	298 930	308 245
R,90,k [N]	83 714	148 799	213 883	278 967	308 245
f,90,k [MPa]	12,1	14,4	15,5	16,2	14,9

KARLSRUHE METHOD WITH THREADED STEEL RODS					
	BFS 2010:2 BKR 13				
Support length	L=60	L=90	L=120	L=150	L=180
N,ki,k [N]	127 483	127 483	127 483	127 483	127 483
c,h [N/mm2]	140,1	140,1	140,1	140,1	140,1
rho,w [kg/m3]	450	450	450	450	450
alpha	1,57	1,57	1,57	1,57	1,57
E,steel [MPa]	210 000	210 000	210 000	210 000	210 000
I,screw [mm4]	552	552	552	552	552
k,c90	1	1	1	1	1
f,yk [MPa]	400	400	400	400	400
f,c90,k [MPa]	8	8	8	8	8
l,screw [mm]	400	400	400	400	400
A,screw [mm2]	83	83	83	83	83
b,beam [mm]	115	115	115	115	115
h,beam [mm]	630	630	630	630	630
l,support [mm]	60	90	120	150	180
l,ef,1 [mm]	90	120	150	180	210
l,ef,2 [mm]	873	903	933	963	993
n	2	4	6	8	10
d,screw [mm]	12	12	12	12	12
d,screw,n [mm]	10,3	10,3	10,3	10,3	10,3
lambda,k	0,511	0,511	0,511	0,511	0,511
N,pl,k [N]	33 329	33 329	33 329	33 329	33 329
k	0,707	0,707	0,707	0,707	0,707
kappa,c	0,837	0,837	0,837	0,837	0,837
R,c,k [N]	27 885	27 885	27 885	27 885	27 885
R,ax,k [N]	54 870	54 870	54 870	54 870	54 870
f,ax,k	-	-	-	-	-
k,d	-	-	-	-	-
n,ef	-	-	-	-	-
R,k [N]	27 885	27 885	27 885	27 885	27 885
l,ef x b x f,c,90,k	82 800	110 400	138 000	165 600	193 200
n x R,k + l,ef x b x f,c,90,k	138 569	221 939	305 308	388 677	472 047
b x l,ef,2 x f,c,90,k	802 919	830 519	858 119	885 719	913 319
R,90,k [N]	138 569	221 939	305 308	388 677	472 047
f,90,k [MPa]	20,1	21,4	22,1	22,5	22,8